The Zymoseptoria tritici avirulence factor AvrStb6 accumulates in hyphae close to stomata and triggers a wheat defense response hindering fungal penetration

Julien Alassimone[1,*], Coraline Praz[2,*], Cécile Lorrain[1], Agustina De Francesco[2], Cristian Carrasco-López[2], Luigi Faino[3], Lukas Meile[2], Andrea Sánchez-Vallet[1,2]

Affiliations:

[1] Plant Pathology, Institute of Integrative Biology, ETH Zürich, Zürich, Switzerland

[2] Centro de Biotecnología y Genómica de Plantas (CBGP/Universidad Politécnica de Madrid-Instituto Nacional de Investigación Agraria y Alimentaria/Centro Superior de Investigaciones Científicas (INIA/CSIC). Campus de Montegancedo. Pozuelo de Alarcón (Madrid) Spain.

Corresponding author: Andrea Sánchez-Vallet: andrea.sanchezv@upm.es

ABSTRACT

Zymoseptoria tritici, the causal agent of septoria tritici blotch, is one of Europe's most damaging wheat pathogens, causing significant economic losses. Genetic resistance is a common strategy to control the disease, *Stb6* being a resistance gene used for over 100 years in Europe. This study investigates the molecular mechanisms underlying Stb6-mediated resistance. Utilizing confocal microscopy imaging, we identified that *Z. tritici* epiphytic hyphae mainly accumulates the corresponding avirulence factor AvrStb6 in close proximity to stomata. Consequently, the progression of AvrStb6-expressing avirulent strains is hampered during penetration. The fungal growth inhibition co-occurs with a transcriptional reprogramming in wheat characterized by an induction of immune responses, genes involved in stomata regulation, and cell wall-related genes. Overall, we shed light on the gene-for-gene resistance mechanisms in the wheat - *Z. tritici* pathosystem at the cytological and transcriptomic level, and our results highlight that stomata penetration is a critical process for pathogenicity and resistance.

Keywords: Plant resistance, wheat fungal pathogen, stomatal-mediated resistance, transcriptomics, gene-for-gene interaction, septoria tritici blotch

INTRODUCTION

Disease outcomes in plant-pathogen interactions are determined by the pathogen's ability to infect a host and the host's capacity to hamper the invader's progression. This intricate interaction forces both organisms to gain novel mechanisms to coexist with each other through evolution (Sacristán and García-Arenal 2008; Krattinger and Keller 2016). The plant immune system protects against invading microorganisms through the activity of resistance genes that recognize specific components of pathogens, while pathogens adapt with numerous infection strategies to circumvent the immune response and successfully colonize the host (Sánchez-Vallet et al. 2018). Host detection of common pathogen molecular patterns triggers an immune response that frequently culminates in the arrest of pathogen progression (Jones and Dangl 2006; Cook et al. 2015; Kanyuka and Rudd 2019). This immune response is counteracted by invading microorganisms through the secretion of so-called effectors (Toruño et al. 2016). Plants have, in turn, evolved to specifically recognize particular forms of these effectors and hinder the pathogen progression. In these cases, effectors are known as avirulence factors, and they are specifically recognized by host resistance proteins in a gene-for-gene manner (Jones and Dangl 2006; Toruño et al. 2016). Although this type of resistance is broadly distributed in plant species, the mechanisms involved in arresting the growth of avirulent strains are frequently unknown.

The fast-evolving pathogen *Zymoseptoria tritici* is the causal agent of septoria tritici blotch (STB) and Europe's most devastating wheat pathogen (Fones and Gurr 2015). STB disease is challenging to control due to the development of fungicide resistance by *Z. tritici* and the erosion of genetic resistance in modern cultivars (Brown et al. 2015;

Torriani et al. 2015; O'Driscoll et al. 2014). Infection of *Z. tritici* is initiated by the germination of the asexual or sexual spores on the leaf surface. Then, the emerging hyphae penetrate the apoplast through stomata and wounds (Kema et al. 1996; Duncan and Howard 2000; Fones et al. 2017; Battache et al. 2022; Bernasconi et al. 2023). Intercellular hyphae of *Z. tritici* invade the leaf tissue without producing symptoms during the first phase of infection that lasts for a minimum of 7 days (Kema et al. 1996; Duncan and Howard 2000; Steinberg 2015). This asymptomatic phase is followed by a necrotrophic phase, which is characterized by the development of chlorotic and necrotic lesions and the production of pycnidia, the asexual reproductive structures (Sánchez-Vallet et al. 2015; Steinberg 2015).

Until now, 21 resistance genes against STB have been mapped to the wheat genome (Brown et al. 2015), three of them (*Stb6*, *Stb16q* and *Stb15*) have been cloned (Saintenac et al. 2018, 2021; Hafeez et al. 2023). These resistance genes generally confer resistance against *Z. tritici* strains that harbor the corresponding avirulence factors. The resistance gene *Stb6*, present in approximately 15% of wheat cultivars, is one of the most frequently used resistance genes in breeding programs (Chartrain et al. 2005; Arraiano and Brown 2006; Brown et al. 2015). Stb6 is a wall-associated kinase (WAK) that recognizes the fungal avirulence factor AvrStb6 (Zhong et al. 2017; Kema et al. 2018; Saintenac et al. 2018). In contrast to what has been described for other pathosystems, *Z. tritici* avirulence factor recognition does not lead to a hypersensitive response (Cohen and Eyal 1993; Kema et al. 1996; Battache et al. 2022). Penetration to the apoplast is crucial for wheat resistance against *Z. tritici*. The wheat resistance gene *Stb16q*, encoding for a cysteine-rich protein kinase, and recognition of the avirulence factor Avr3D1 prevent *Z. tritici* penetration through the stomata (Saintenac et al. 2021;

Battache et al. 2022; Meile et al. 2023). In addition, it was recently demonstrated that stomatal closure is associated with Stb16q- and Stb6-mediated resistance (Battache et al. 2022; Ghiasi Noei et al. 2022) and that wounding partially enables infection by avirulent strains (Battache et al. 2022; Bernasconi et al. 2023). A better understanding of Stb6-mediated resistance mechanisms against *Z. tritici* invasion would provide us with novel tools to improve control methods against *Z. tritici*. In this study, we demonstrated that AvrStb6 is accumulated in hyphae penetrating the stomata where the progression of avirulent strains is hindered. We characterized the specific transcriptional reprogramming occurring in the host upon recognition of AvrStb6 making use of isogenic lines of *Z. tritici* expressing or not *AvrStb6* and the purified protein AvrStb6. We showed that AvrStb6 recognition triggers the induction of genes involved in stomatal closure regulation and a defense response associated with the pathogen's incapacity to colonize and infect the plant.

RESULTS

Stomatal penetration is hindered in incompatible interactions.

To investigate at which infection stage AvrStb6 recognition hinders *Z. tritici* progression, we monitored the colonization of Chinese Spring (with Stb6) leaves by fluorescently labeled strains that either harbor a virulent or an avirulent allele of *AvrStb6* (strains 3D7 and 1E4, respectively; Figure 1). Successful penetration events of the virulent strain were observed as early as 6 dpi (Figure 1A and G). At that stage, hyphae of both strains colonized the leaf surface and were frequently in contact with stomata. Hyphae from the virulent strain penetrated the substomatal cavity and

colonized the stomata proximate intercellular space. At 10 and 14 dpi, hyphae of the virulent strain thoroughly colonized the apoplast and the substomatal cavity (Figure 1B and C). In contrast, the avirulent strain was incapable of entering the stomata and remained on the leaf surface at the three observed time points (Figure 1E and F). Only in extremely rare events, we observed severely limited hyphal growth of avirulent strains inside the leaves (Supplementary Figure S2). Overall, our results suggest that stomata act as a main barrier for AvrStb6-expressing avirulent strains and that AvrStb6 recognition occurs at or in close proximity to the stomata.

We corroborated the penetration capacity of avirulent strains by infecting wheat cultivar Chinese Spring with 3D7-GFP and a mutant line ectopically expressing the avirulent effector gene *AvrStb6*$_{1E4}$. The lines expressing *AvrStb6*$_{1E4}$ were impaired in stomatal penetration, while the control lines colonized the apoplast. These results demonstrate that AvrStb6 recognition prevents stomatal penetration (Supplementary Figure S3A-F). Additionally, to demonstrate the role of Stb6, we assessed stomatal penetration of the avirulent strain 1E4 in wheat near-isogenic lines (NILs) with and without *Stb6* in the Bobwhite background (Saintenac et al. 2018). Only *Stb6*-harboring wheat lines prevented penetration of 1E4 (Supplementary Figure S3G-L). These results demonstrated that AvrStb6-Stb6 interactions result in the pathogen being mostly unable to enter the leaf via the stomata.

The avirulence factor AvrStb6 is expressed during stomata penetration and apoplast colonization.

Although *AvrStb6* has been described to exhibit a peak of expression at the onset of the necrotrophic phase (Rudd et al. 2015; Zhong et al. 2017), its protein accumulation

pattern at the cellular level remains undetermined. We used a 3D7 mutant expressing AvrStb6$_{1E4}$-GFP to monitor the cell-specific accumulation of AvrStb6 during colonization of the wheat NILs (with or without *Stb6;* Figure 2 and Supplementary Figure S4). In addition, this *Z. tritici* reporter strain constitutively expresses cytosolic mCherry, allowing the visualization of hyphae colonizing wheat plants in microscopy assays. Regardless of the presence of *Stb6* in the host, epiphytic hyphae accumulated AvrStb6$_{1E4}$-GFP mainly in hyphal cells in direct contact with stomata, and no signal was detected on the remaining hyphae at the leaf surface (Figure 2A, Supplementary Figure S4). In the compatible interaction, hyphae growing in the apoplast also exhibited a substantial accumulation of AvrStb6$_{1E4}$-GFP (Figure 2B, Supplementary Figures S4B and D). These results indicate a cell-specific accumulation of AvrStb6$_{1E4}$-GFP at the penetration sites and in the apoplastic space. This specific protein accumulation pattern is in accordance with the previously described tight *AvrStb6* gene expression pattern (Meile et al. 2018). During epiphytic growth, *AvrStb6* promoter activation was mostly restricted to fungal cells in direct contact with stomata and some of the hyphae extremities (Supplementary Figure S4K) (Meile et al. 2020). However, *AvrStb6* promoter activation was observed in all hyphae colonizing the apoplast (Supplementary Figure S4L) (Meile et al. 2020). These and our previously published results (Meile et al. 2020) demonstrate that transcription of *AvrStb6* is tightly regulated at the cellular level, and that the protein accumulation occurs on the site of *Z. tritici* colonization. We therefore hypothesize that the role of AvrStb6 is specifically related to the host invasion.

Z. tritici AvrStb6 is a secreted protein.

148 The avirulence factor AvrStb6 has a predicted signal peptide, suggesting that it is
149 secreted (Brunner and McDonald 2018; Stephens et al. 2021) (Figure 3A). Interestingly,
150 upon stomatal contact, AvrStb6$_{1E4}$-GFP does not fully co-localize with the cytosolic
151 reporter mCherry and seem to be located at *Z. tritici* cell surface or cell wall (Figure
152 3B). To test whether AvrStb6 is secreted from fungal cells and whether it remains
153 bound to the fungal cell wall, we grew the 3D7 ectopic mutant lines expressing the
154 GFP-tagged virulent and avirulent *AvrStb6* alleles (*AvrStb6*$_{3D7}$-GFP and *AvrStb6*$_{1E4}$-GFP,
155 respectively) in axenic liquid media. We evaluated the presence of AvrStb6-GFP both in
156 the spent medium and in the fungal cell by Western blot. As a control, we used a
157 reporter 3D7 strain expressing cytosolic GFP. As expected, the cytosolic GFP was
158 mainly present in the cell fraction (pellet). In contrast, both isoforms of AvrStb6-GFP
159 (AvrStb6$_{1E4}$-GFP and AvrStb6$_{3D7}$-GFP) were predominantly present in the culture
160 medium (Figure 3C). The protein detected in the pellet was minor, regardless of the
161 treatment with urea, a cell disruptive agent. These results demonstrate that AvrStb6
162 has a functional signal peptide that enables the secretion of the effector protein and
163 supports its extracellular function.

164 **AvrStb6 triggers an immune response in resistant wheat cultivars.**

165 To determine the host transcriptomic response to AvrStb6 recognition, we compared
166 the transcriptomic profiles of leaves infiltrated with a purified AvrStb6 protein
167 (avirulent isoform) and of leaves infected with a strain of *Z. tritici* expressing the
168 avirulent isoform of AvrStb6. We infiltrated the *Pichia*-produced avirulent isoform of
169 AvrStb6 (Supplementary Figure S5) into leaves of cultivar Chinese Spring and
170 performed RNA sequencing of the leaves after 1, 2, and 5 hours post-infiltration.

Phosphate-buffered saline (PBS) infiltration was used as control. The purified avirulent isoform of AvrStb6 protein did not produce any visible symptoms in wheat leaves and was shown to be recognized by Chinese Spring since its infiltration prior to the infection with the virulent strain 3D7 led to a reduction of virulence (Figure 4A). In addition, we determined the transcriptomic response of the same resistant cultivar (Chinese Spring) upon infection with *Z. tritici* wildtype strain (3D7) and with a mutant line expressing the avirulent allele of *AvrStb6* (3D7+AvrStb6$_{1E4}$) at 3 and 6 dpi. To visualize the overall changes in the host transcriptome upon infection or protein infiltration, we performed a multidimensional scaling (MDS) on the expression data of the 33,249 expressed genes. The MDS showed that samples clustered according to experiments (*Z. tritici* infection assay vs AvrStb6-infiltration experiment, first dimension) and to timepoints of the spray inoculation experiment (second dimension; Supplementary Figure S6A). When the MDS was performed for each experiment separately, the data clustered according to the timepoints and the treatments (Supplementary Figure S6B and C). The MDS analysis indicated that AvrStb6-triggered transcriptomic reprogramming changes over time.

We first analyzed the transcriptomic response of wheat upon infiltration with the avirulent isoform of AvrStb6 protein. We performed differential gene expression analyses on the control plants (infiltrated with PBS) and AvrStb6-infiltrated plants at each timepoint (Supplementary Table S5). We identified 421, 2475, and 1883 differentially expressed genes (DEGs) at 1, 2, and 5 hpi, respectively, resulting in 3385 genes that are differentially expressed (DE) upon AvrStb6 infiltration at least at one timepoint (hereafter called “DEGs in infiltration”, Figure 4B and Supplementary Table S4). Out of these 3385 genes, 259 are differentially expressed at all the three

timepoints and 876 at two timepoints. The results suggest that AvrStb6 triggered distinct waves of differentially regulated genes, most of them being upregulated (Figure 4C). DEGs after AvrStb6 infiltration were enriched in "calcium ion transmembrane transport", "oxylipin biosynthetic process" Gene Ontology (GO) terms and other GO terms linked to biotic stress responses, photosynthesis, and cell wall-related terms (Supplementary Figure S7 and Table S6, "DEGs in infiltration"), suggesting that cell wall remodeling and immune response induction are key parts of the host response against AvrStb6. Remarkably, we identified several up-regulated genes involved in stomatal closure, i.e., seven genes encoding for putative *Respiratory Burst Oxidases* (*RBOH*), an *Open Stomata1* (*OST1*, protein kinase mediating the regulation of stomatal aperture/closure), 1 *Serine/threonine-protein kinase PBL27*, 4 *Calcium-Dependent Protein Kinase* (*CPK*), 1 *Aluminum-Activated, Malate Transporter 12* (*ALMT12*) and a Serine/threonine-protein kinase *Botrytis-induced Kinase1* (*BIK1*) homologs (Mustilli et al. 2002; Kwak et al. 2003; Geiger et al. 2010; Meyer et al. 2010; Sasaki et al. 2010; Brandt et al. 2012; Scherzer et al. 2012; Kadota et al. 2014; Zheng et al. 2018; Liu et al. 2019) (Figure 4D; Supplementary Table S7). These results suggest that wheat response to AvrStb6 infiltration may trigger Reactive Oxygen Species (ROS) accumulation and stomatal closure.

Second, we analyzed the transcriptome of wheat plants infected with the virulent strain 3D7 and the avirulent strain 3D7+AvrStb6$_{1E4}$. In total, 4049 and 1713 genes were differentially expressed upon infection with the virulent strain 3D7 compared to the control treatment (mock) at 3 and 6 dpi, respectively (Figure 4E; Supplementary Table S5). In plants infected with the avirulent strain expressing AvrStb6 (3D7+AvrStb6$_{1E4}$), 4375 and 2049 genes were differentially expressed from the control at 3 and 6 dpi,

respectively (Figure 4E, and Supplementary Tables S4 and S5). We identified 3 distinct sets of differentially expressed genes: i) the "core DEGs" consisted of 2813 genes differentially expressed upon infection with both strains compared to the control at each timepoint (grey in Figure 4F); ii) the "3D7-specific DEGs" consisted of 843 genes differentially expressed exclusively upon infection with the virulent strain (green in Figure 4F); and iii) the "3D7+AvrStb6$_{1E4}$-specific DEGs" were differentially expressed only upon infection with the AvrStb6-expressing strain, but not with the wild-type strain regardless of the timepoint (1618 genes, orange in Figure 4F). We performed a GO enrichment analysis in these three sets of genes to get insights into the function of the DEGs. We observed enrichment in core DEGs in GO terms linked to stress response and plant cell wall. We observed an enrichment in the "calcium ion transmembrane transport", "oxylipin biosynthetic process", "cellulose synthase" and "plant cell wall biogenesis" GO terms and in GO terms linked to photosynthesis only in the 3D7+AvrStb6$_{1E4}$-specific DEGs (Supplementary Figures S7-S9). Within the 3D7+AvrStb6$_{1E4}$-specific DEGs, up-regulated genes involved in stomatal closure regulation, including *Slow Anion Channel-associated1* (*SLAC1*), 2 *RBOH,* and 3 *CPKs* homologs were identified (Kwak et al. 2003; Negi et al. 2008; Vahisalu et al. 2008; Geiger et al. 2010; Brandt et al. 2012; Scherzer et al. 2012). In accordance with the previous findings with AvrStb6 protein, we conclude that recognition of the avirulent strain induces a transcriptomic reprograming involved in stomatal closure (Figure 4G; Supplementary Table S7).

Finally, the specific response to AvrStb6 was determined by combining the protein infiltration and infection results. Around 53% of the DEGs upon infiltration with the avirulent version of AvrStb6 protein were also differentially expressed in the presence

of *Z. tritici* (1798 out of 3385 genes for the case of the avirulent strain, Figure 5A, B), highlighting that the direct infiltration of one single avirulence factor highly mimics the infection response in wheat. To determine the response triggered specifically upon AvrStb6 recognition, we identified 247 genes that were differentially expressed in the presence of AvrStb6 both when the avirulent version of AvrStb6 protein was applied ("DEGs in infiltration") and when the plants were infected with the AvrStb6-expressing strain, but not with the virulent strain. These 247 genes were referred to as "AvrStb6 response" (Figure 5A, B). Of these, 103 and 76 genes were up-regulated and down-regulated, respectively, upon infection with the avirulent strain at 3 dpi. We checked the Uniprot annotation and blasted the protein sequences of all those 247 genes against the NCBI conserved domain database (Supplementary Table S8). Among the up-regulated genes upon infection by 3D7+AvrStb6 strain at 3 dpi that were also up-regulated upon AvrStb6 infiltration (Supplementary Table S9 and S10), we identified genes encoding for an MLO (Mildew resistance locus o)-like protein, for 1 chitinase domain-containing protein, for 2 NOD-like receptors (NLRs), for 1 putative receptor-like proteins (RLP) and for 24 putative receptor-like kinases (RLKs). Among the RLKs, 2 harbored a lectin-like domain, 17 a leucine-rich repeat (LRR) domain, 1 a jacalin-like protein kinase and 4 a wall-associated kinase (WAK) domain (Supplementary Table S9, highlighted in light green). Expression levels of some of these genes are shown in Figure 5C (Supplementary Table S10; highlighted in dark green). The previously cloned resistance genes *Stb6*, *Stb15* and *Stb16q* were up-regulated upon AvrStb6 treatment, and upon the infection by the avirulent strain and the virulent strain (Supplementary Table S4, in red, green and blue, respectively). Therefore, although these well-characterized resistance genes are up-regulated upon AvrStb6 recognition

(Set_DEG_INF_all), they were not considered to be part of the AvrStb6-specific response. We additionally identified several up-regulated genes upon AvrStb6 infiltration and infection with the avirulent strain encoding proteins involved in cell wall modification, including 1 glycosyltransferase, 1 pectin esterase, 2 glucan endo-1,3-beta-D-glucosidases, and an alpha-L-fucosidase (Supplementary Table S9, highlighted in orange). Moreover, we identify some putative genes encoding proteins playing a role in stomatal movement, including two CBL-interacting protein kinase (CIPKs), a sugar transporter protein (STP), and a plant glutamate receptor (GLR) homolog (Kong et al. 2016; Förster et al. 2019; Flütsch et al. 2020) (Figure 6B; Supplementary Table S9, highlighted in blue). These results suggest that the specific response triggered upon AvrStb6 recognition involves a transcriptomic reprogramming characterized by the induction of defense-, stomatal closure-, and cell wall-related genes.

Transcriptomic pattern of *Z. tritici* avirulent strains.

We finally analyzed the transcriptomic pattern of virulent and avirulent *Z. tritici* strains during infection and showed that data clustered based on timepoint and genotype (Figure 6A). Remarkably, no major changes were identified in the transcriptome of the avirulent strain 3D7+AvrStb6$_{1E4}$ between the two timepoints analyzed (Figure 6B and C and Supplementary Table S11). Thirteen genes were differentially expressed between 3D7 and 3D7+AvrStb6$_{1E4}$ at 3 dpi and 139 at 6 dpi (Figure 6B). By comparing the lists of DEGs, we noticed that most of the genes (82%) that were differentially expressed between the two timepoints in 3D7 were also differentially expressed between the two strains at 6 dpi, suggesting that both strains have a similar transcriptomic profile at 3 dpi, but at later stages 3D7 transcriptomic profile changes, consistent with its

successful host colonization (Figure 6C). We then analyzed the sequences of all the DEGs in *Z. tritici* for putative effector genes. Around 60% of the differentially expressed genes between both isolates were secreted, and more than 40% were putative effector genes (Figure 6D). The results indicate that the immune response triggered in wheat plants upon AvrStb6 recognition does not induce detectable changes in the transcriptome of *Z. tritici*.

DISCUSSION

Resistance towards fungal pathogens features the specific recognition of avirulence factors, which prevents the progression of the infection. However, the mechanisms involved in arresting the growth of the avirulent strain remain largely unknown. In this work, we provide a better understanding of the intricate mechanisms that are involved in strain-specific resistance against the major wheat pathogen *Z. tritici*. We demonstrated that an accumulation of AvrStb6 effector occurs during penetration of the pathogen through the stomata. At this stage, the pathogen progression is arrested in resistant wheat cultivars harbouring Stb6. We propose that AvrStb6 triggers a rapid induction of wheat defense, cell wall-related genes, and genes involved in stomatal closure, contributing to preventing host colonization of the avirulent strain and its penetration through the stomata.

Z. tritici has an extended asymptomatic phase considered critical for the outcome of the infection (Sánchez-Vallet et al. 2015; Steinberg 2015). During this phase, *Z. tritici* spores germinate, hyphae grow epiphytically on the leaf surface, penetrate through the stomata or wounds, and grow in the apoplastic space (Kema et al. 1996; Duncan

and Howard 2000; Fones et al. 2017; Haueisen et al. 2019; Battache et al. 2022). The cytological analysis carried out in this work enabled us to identify the stomata as key for the infection process, not only because it is the most frequent gate for fungal penetration (Kema et al. 1996; Duncan and Howard 2000; Fones et al. 2017), but also since it is where fungal cells accumulate AvrStb6, a critical avirulence factor, and where the growth of avirulent strains is arrested. Indeed, we observed that epiphytic hyphae produce very low levels of AvrStb6, while cells attempting to penetrate the stomata accumulate AvrStb6. Once the virulent strains entered the substomatal cavity and colonized the apoplast, AvrStb6 levels remained high. These results are in accordance with the reported gene expression pattern of *AvrStb6* (Meile et al. 2020) and are similar to the one described for another avirulence gene, *Avr3D1* (Meile et al. 2023). Previously published transcriptomic analyses showed that both effector genes (*AvrStb6* and *Avr3D1*) were induced at the onset of the necrotrophic phase (Rudd et al. 2015; Palma-Guerrero et al. 2017; Zhong et al. 2017; Meile et al. 2018). However, literature (Meile et al. 2020, 2023) and our microscopic analysis indicate that these two effectors are induced much earlier during the infection. We hypothesize that other effector genes with similar expression patterns (Rudd et al. 2015; Palma-Guerrero et al. 2017; Haueisen et al. 2019) could also be activated during penetration and remain relatively high during growth in the apoplast.

Taken together, the restricted expression pattern of *AvrStb6*, the observed AvrStb6 accumulation in fungal cells close to stomata, and the blockage of AvrStb6-expressing strains at the level of the stomata indicate that AvrStb6 is recognized during stomatal penetration. Plants regulate stomatal opening upon a pathogen attack to prevent penetration by those pathogens that use natural openings, indicating that pathogen

337 detection through stomata is a general defensive strategy (Melotto et al. 2017; Wu
338 and Liu 2022). Noticeably, it was recently reported that AvrStb16 and Avr3D1
339 recognition also block avirulent isolates during wheat invasion through stomata and
340 that wheat stomata were closed following recognition of *Z. tritici* strains expressing
341 AvrStb16 or AvrStb6 (Saintenac et al. 2021; Battache et al. 2022; Ghiasi Noei et al.
342 2022; Meile et al. 2023). We propose that AvrStb6 recognition occurs at the stomata
343 and that resistance proteins recognizing Avr3D1, AvrStb6 and AvrStb16 are expressed
344 in both guard cells and subsidiary cells. We identified several genes involved in
345 stomatal closure that were upregulated upon AvrStb6 treatment and upon infection
346 with the avirulent strain, including seven homologs of RBOH, 1 homolog of BIK1, 2
347 homologs of PBL27, 3 homologs of CPK, 1 homolog of OST1, 1 homolog of ALMT12,
348 and 1 homolog of SLAC1 (Mustilli et al. 2002; Kwak et al. 2003; Negi et al. 2008;
349 Vahisalu et al. 2008; Geiger et al. 2010; Meyer et al. 2010; Sasaki et al. 2010; Brandt et
350 al. 2012; Scherzer et al. 2012; Kadota et al. 2014; Zheng et al. 2018; Liu et al. 2019).
351 These results suggest that stomatal closure triggered by the avirulent strain and
352 AvrStb6 treatment could be due to recognition by transmembrane receptors that, in
353 turn, could activate NADPH oxidases, protein kinases, and anion channels to initiate a
354 ROS burst and promote stomatal closure.

355 Our transcriptomic analysis, which combines the treatment with AvrStb6 protein and
356 the infection with isogenic *Z. tritici* lines with and without *AvrStb6*, revealed the
357 specific transcriptomic response upon recognition of this avirulence factor. Among the
358 genes differentially expressed upon AvrStb6 infiltration and infection with the
359 avirulent strain, cell wall-related GO terms were enriched. We hypothesize that
360 changes in the cell wall triggered by recognition of the avirulence factor result in

arresting fungal growth, as shown in other pathosystems (Menna et al. 2021; Molina et al. 2021). However, we cannot discard that AvrStb6 function involves targeting the cell wall independently of the immune response triggered upon its recognition. We identified several resistance-related genes up-regulated upon infection by the avirulent strain and treatment with the avirulence factor. In particular, we identified 24 RLKs and 1 RLPs which are known to be crucial for plant immunity (Tang et al. 2017). Remarkably, the resistance genes *Stb6*, *Stb16q,* and *Stb15* were up-regulated upon AvrStb6 infiltration and infection with the virulent and avirulent strains of *Z. tritici*, suggesting that the resistance genes are induced during wheat infection (Bernasconi et al. 2023) but also upon recognition of AvrStb6.

The dual transcriptomic approach simultaneously determined the response triggered in the plant and its effect on the pathogen. Our results showed that the virulent and avirulent strains harbor different acclimation strategies to the host at the transcriptomic level. At an early timepoint (3 dpi), both the virulent and avirulent hyphae mostly grow epiphytically. Accordingly, at this timepoint, only 13 genes were differentially expressed between the virulent and the avirulent strain, of which 6 were predicted to be effectors. At a later timepoint (6 dpi), the virulent strain colonizes the apoplast. However, the avirulent strain remains blocked on the leaf surface. This translates into a new set of genes induced in 3D7 that remain unchanged in the avirulent strain. Among this new set of genes, 58 are predicted to encode putative effectors and are probably involved in penetration or apoplast colonization of virulent strains. We expected an induction of stress-related genes in the avirulent strain, but we were not able to detect a transcriptomic reprogramming. We hypothesize that this lack of transcriptomic response is due to the fact that the defense response only

385 impacts upon specific fungal cells (e.g. cells attempting to penetrate), and that this
386 response was not detected in the whole leaf transcriptomic approach undertaken in
387 this study. Alternatively, the observed phenotype might indicate that *Z. tritici* does not
388 undergo a strong stress response upon recognition.

389 **Conclusions**

390 This work describes how gene-for-gene resistance acts in wheat against the major
391 pathogen *Z. tritici*. Our results shed light on the resistance response triggered upon
392 pathogen recognition and suggest that cell wall modifications might play a key role.
393 Furthermore, we provided evidence for the capacity of fungal strains to sense the
394 apoplast and/or the stomata to produce effector proteins. Finally, our data
395 demonstrate that recognition of avirulent strains prevents their penetration through
396 the stomata and, subsequently, apoplast colonization.

397

398 **MATERIALS AND METHODS**

399 **Plant and Fungal material.**

400 Wheat seeds (*Triticum aestivum*) of cultivars Chinese Spring and Runal were provided
401 by DSP Ltd. (Delley, Switzerland). Seeds of the 2 Bobwhite near-isogenic lines
402 (Bobwhite, Bobwhite + Stb6 T2-19-2, and Bobwhite + Stb6 T2-41-2) (Saintenac et al.
403 2018) were kindly provided by Kostya Kanyuka and bulk-amplified in our greenhouse
404 facility (16h photoperiod, 70% humidity, 18°C during the day and 15°C at night). For all
405 experiments described in this study, wheat seeds were grown in square pots (11 x 11 x
406 12 cm; about 11 plants per pot) containing the peat substrate Jiffy GO PP7 (Jiffy

Products International, Moerdijk, the Netherlands). Plants were grown on a 16h photoperiod at 18°C (day) and 15°C (night) with 80% humidity and 30 klx.

All *Zymoseptoria tritici* strains used in this study were derived from the Swiss isolates ST99CH_3D7 and ST99CH_1E4 (abbreviated as 3D7 and 1E4, respectively) (Linde et al. 2002; Zhan et al. 2002). The reporter lines 3D7-GFP, 3D7-mCherry, 1E4-GFP, and 3D7-mTurquoise + p*AvrStb6*$_{1E4}$::*His1-mCherry* were previously described (Meile et al. 2020; Barrett et al. 2021). Strains expressing AvrStb6 variants (AvrStb6$_{1E4}$, AvrStb6$_{1E4}$-GFP, and AvrStb6$_{3D7}$-GFP) were engineered specifically for this study as described below. *Z. tritici* blastospores were grown in 50ml liquid cultures with yeast-sucrose broth medium (YSB; 10 g L^{-1} yeast extract, 10 g L^{-1} sucrose) or on solid yeast malt agar medium (YMA; 4 g L^{-1} yeast extract, 4 g L^{-1} malt extract, 4 g L^{-1} sucrose, 12 g L^{-1} agar), in the dark, at 18°C. Culture media were supplemented with 50 µg mL^{-1} kanamycin sulfate. Liquid cultures were grown with agitation (250 rpm). *Escherichia coli* and *Agrobacterium tumefaciens* were grown in Luria-Bertani medium (LB; 5 g L^{-1} yeast extract, 10 g L^{-1} tryptone, 10 g L^{-1} NaCl, pH7.5) supplemented with 50 µg mL^{-1} kanamycin sulfate or with a combination of 50 µg mL^{-1} kanamycin sulfate, 100 µg mL^{-1} carbenicillin and 50 µg mL^{-1} rifampicin, respectively. LB was supplemented with 10 g L^{-1} agar when used as solid media. *E. coli* and *A. tumefaciens* were grown in the dark at 37°C and 28°C, respectively. All strains are listed is Supplementary Table S1

Establishment of *Z. tritici AvrStb6* reporter lines.

The reporter line ectopically expressing *AvrStb6* from the avirulent strain 1E4 (*AvrStb6*$_{1E4}$), under the control of its native promoter and terminator regions (1010 and 1009 bp upstream and downstream of *AvrStb6*$_{1E4}$ coding sequence, respectively),

was obtained by transforming 3D7-GFP (Barrett et al. 2021) with the vector pES1_Avr1E4 previously described (Zhong et al. 2017). To obtain the strains expressing AvrStb6 fused to the Green Fluorescent Protein (GFP) reporter ($AvrStb6_{1E4}$-GFP and $AvrStb6_{3D7}$-GFP), 2 plasmids containing the *AvrStb6* promoter (1009 bp), the open reading frame (ORF) without the stop codon, and the terminator region (1010 bp) of 1E4 and 3D7, respectively, were engineered. 3D7 and 1E4 sequences were amplified from pES1_Avr1E4 (Zhong et al. 2017) and 3D7 genomic DNA, respectively. The *Z. tritici* codon-optimized GFP was amplified from pCeGFP (Kilaru et al. 2015) using NEB Phusion polymerase (New England Biolabs) and the primers listed in Supporting Information Supplementary Table S2. A linker (GGSGGGSG) was integrated between *AvrStb6* and *GFP*. PCR products were purified using the NucleoSpin Gel and PCR Clean-up kit (MACHEREY-NAGEL) and introduced into linearized (with KpnI) pCGEN (Motteram et al. 2011) using the In-Fusion HD Cloning Kit (Takara Bio). The resulting vectors, JA031_pCGEN_p1E4-1E4-GFP-t1E4 and JA035_pCGEN_p3D7-3D7-GFP-t3D7 (Genebank files available in doi: 10.3929/ethz-b-000641399), were used to transform chemically competent *E. coli* HST08 (Stellar competent cells, Takara Bio). Verified plasmids using Sanger sequencing were electroporated into *A. tumefaciens* AGL1 cells and were used to transform the *Z. tritici* reporter line 3D7-mCherry (Barrett et al. 2021). *A. tumefaciens*-mediated transformation was performed as described previously (Meile et al. 2018). Insertions were confirmed by Sanger sequencing. Transgene copy numbers were assessed by quantitative PCR (qPCR), using primers specific for the resistance marker gene (hygromycin B phosphotransferase gene, *hph*, for the untagged *AvrStb6* transformant and neomycin resistance gene, *neo*, for *AvrStb6-GFP* transformants) and the reference gene *TFIIIC1* (*Mycgr3G110539*).

Quantitative PCRs were performed on Roche LightCycler480 following the HOT FIREPol EvaGreen qPCR recommendations (primers listed in Supplementary Table S2). Only transformants with a single transgene insertion were selected for further analysis. We confirmed that the fused proteins were functional since the lines expressing *AvrStb6*$_{1E4}$*-GFP* were avirulent in the cultivar Chinese Spring, but not in the susceptible cultivar Drifter (Supplementary Figure S1).

Infection assays.

Plants were sprayed with a suspension of 10^6 spores mL^{-1} in 0.1% Tween 20 until run-off following the procedure described (Meile et al. 2018). For mock treatments, plants were sprayed with a 0.1% Tween 20 solution. For symptom quantification, second or third leaves were mounted on paper sheets, scanned with a flatbed scanner (CanoScan LiDE 220), and analyzed following the method described in (Zenkl et al. 2023). Data analysis and plotting were performed using RStudio 2023.06.1+524 (RStudio 2020).

AvrStb6 protein secretion assay.

Z. tritici strains expressing either *AvrStb6*$_{1E4}$*-GFP* or *AvrStb6*$_{3D7}$*-GFP* were grown in liquid medium, as mentioned in the fungal material section. Seven days after inoculation, the axenic cultures were filtered through 2 layers of sterile cheesecloth and pelleted (3273 g, 15 min, 4°C). Supernatants (SN) were filtered using 0.2-µm filters, lyophilized and resuspended in 1.5 ml Tris-buffered saline (TBS; 25 mM Tris, 150 mM NaCl, pH 7.5) before aliquoting (60 µL) and stored at -80°C until further experiments ("Filtered SN"). Pellets were washed four times with sterile deionized water and resuspended in 10 ml breaking buffer (BB; 50 mM sodium phosphate, 1 mM phenylmethylsulfonyl fluoride, 1 mM EDTA, 5% glycerol, pH 7.4). Cells were pelleted

again (10 min, 3000 g, 4°C) and resuspended in BB to reach an OD_{600} of 100. An equal volume of glass beads was added to the samples before proceeding with 8 cycles of 30 seconds of vortex homogenization followed by 30 seconds on ice. Samples were then centrifuged at 12000 g for 10 min, and the collected supernatant corresponded to the "Washed pellets" without urea samples, and the remaining pellet was treated with urea. Pellets were resuspended in 10 mL fresh BB supplemented with 6 M urea, and the same procedure was applied (starting from the vortex/ice cycles) to obtain the "Washed pellets" with urea samples. Immunoprecipitation of the samples was performed following the GFP-Trap_MA protocol (Chromotek) using 6 µL of beads per sample and equilibrating the samples with 1.5 volumes of GFP-Trap_MA wash buffer. Elution was done in 2x Laemmli Buffer (125 mM Tris Base, 4% SDS, 20% glycerol, 10% 2-mercapto-ethanol, 2mg mL^{-1} Bromophenol blue).

Protein production in *Pichia pastoris*.

The recombinant protein $AvrStb6_{1E4}$, tagged with a C-terminal c-myc epitope and a polyhistidine (6xHis) tag was purified using the *Pichia pastoris* heterologous expression system. The *$AvrStb6_{1E4}$* coding sequence lacking its endogenous signal peptide was amplified from 1E4 cDNA and pPICZalphaB (Invitrogen) was linearized using an inverse PCR approach. Amplifications were performed using NEB Phusion polymerase with the primers listed in Supplementary Table S2, gel-purified with the NucleoSpin Gel and PCR Clean-up kit (MACHEREY-NAGEL) and assembled using the In-Fusion HD Cloning Kit (Takara Bio). After Sanger sequencing validation, the resulting vector (pPICZalphaB_AvrStb6_1E4; Genebank file available in supplementary files) was used

for transformation of *Pichia pastoris* strain X-33, which was cultured according to the *Pichia* Expression Kit manual (K1710-01, Invitrogen).

P. pastoris preculture was prepared in 250 ml yeast extract peptone dextrose (YPD; 1% yeast extract, 2% peptone, 2% dextrose) media at 28°C, 250 rpm, until reaching an OD_{600} of between 2 and 6 (for 16-18 h). The preculture was pelleted at 3000 g for 5 min, the cells were resuspended in buffered glycerol-complex medium (BMMY; 1% yeast extract, 1% peptone, 100 mM potassium phosphate, pH 6, 1.34% yeast nitrogen base medium, $4x10^{-5}$ % biotin, 1% methanol) to a final OD_{600} of 1, divided in eight 250mL cultures (grown in 1L sterile Erlenmeyer) and grown for 29 h at 28°C and shaking at 265 rpm. Methanol was added to a final concentration of 0.5% after 24 h. The supernatant of the culture was centrifuged at 13689 g for 4 min at 4°C. For AvrStb6 purification, we followed the HisPur Ni-NTA resin batch protocol (Thermo Scientific). Ni-NTA-bound AvrStb6 was eluted in phosphate-buffered saline (PBS; 20 mM sodium phosphate, 300 mM sodium chloride pH 7.4) supplemented with 250 mM imidazole. Imidazole was eliminated from elution fractions by buffer exchange using PBS and illustra NAP-25 columns (GE Healthcare). The presence of purified protein in the elution fractions was confirmed by western blot analysis using anti-HA antibodies (western blot analysis details below). The concentration of the purified protein was estimated by measuring the 280-nm absorbance and accounting for the cysteine reductions. To evaluate the functionality of the purified $AvrStb6_{1E4}$, we infiltrated 13 days post germination (dpg) Chinese Spring second leaves with either the purified $AvrStb6_{1E4}$ recombinant protein at a concentration of 176 mg mL^{-1} (23 leaves) or PBS (21 leaves). Subsequently, plants were spray-inoculated with 3D7 or with a mock

522 treatment as described in the infection assay section. Second leaves were harvested 11
523 days after infection for symptom evaluation.

524 **SDS-PAGE, western blots, and Coomassie analysis.**

525 Protein samples were separated by SDS-PAGE and transferred to a polyvinylidene
526 fluoride (PVDF) membrane (TurboMidi 0.2 µm PVDF membrane; BioRad) using the
527 Trans-Blot Turbo system (Bio-Rad). Membranes were blocked at room temperature
528 (RT) in blocking buffer (PBS, 0.01% Tween 20, 4% BSA) and incubated in a primary
529 antibody solution anti-GFP-HRP (1/5000, MACS Miltenyi Biotec) and 1/5000 anti-His
530 (11667475001, Roche) for GFP and His-Tag detection, respectively) followed by
531 incubation with anti-mouse IgG (1/10000). SuperSignal West Pico Chemiluminescent
532 Substrate kit (Thermo Scientific) was used for immunodetection. Blotted membranes
533 were stained with Coomassie staining solution (10% acetic acid, 45% EtOH, 0.1%
534 Brillant blue R, 20 min, RT). Image acquisition was performed on a ChemiDoc Imaging
535 System (Bio-Rad).

536 **Confocal laser scanning microscopy.**

537 Second leaves of infected and mock-treated plants were harvested immediately before
538 observation. The top 3 cm of each leaf were discarded, and the adaxial side of the
539 adjacent section of approximately 2 cm was observed in 0.02% Tween 20 solution.
540 Propidium iodide (PI) staining was performed by soaking the leaf sections in 0.02%
541 Tween 20 solution amended with 10 µg mL^{-1} PI and applying vacuum. Images were
542 acquired using an inverted Zeiss LSM 780 confocal microscope. Images of the *AvrStb6*
543 promoter activity were acquired as described (Meile et al. 2020). All other images were
544 acquired using two excitation sources, a diode-pumped solid-state laser (DPSSL; 561

nm) and an argon (488 nm) laser using the following detection settings: 494.95-535.07 nm for GFP signal, 623.51-641.26 nm for mCherry signal, 656.01-681.98 nm for the chloroplast autofluorescence, and 596.87-632.38 nm to detect PI signal. Images were processed using the Fiji platform of ImageJ (Schneider et al. 2012). Image processing included brightness and contrast adjustments, median filters (radius of 1 pixels), generation of maximum intensity z-projection, orthogonal projections, cropping, and addition of scale bars.

Plant inoculation, tissue harvest, and RNA sequencing.

Chinese Spring wheat plants (12 days post sowing) were treated with 3D7-GFP, 3D7-GFP expressing *AvrStb6*$_{1E4}$ (3D7-GFP+*AvrStb6*$_{1E4}$) or mock solution (0.1% (v/v) Tween 20 solution), as described for the infection assays. Samples were collected at 3 and 6 days post infection (dpi). For each treatment, the top 3 cm from the leaf tips were discarded, three second leaves (from independent plants) were pooled and flash-frozen in liquid N_2. Concurrently, 13-day old Chinese Spring leaves were infiltrated with 176 mg mL^{-1} of AvrStb6 purified protein (see Protein production in *P. pastoris*) or with PBS buffer. Infiltrated areas were marked and collected at 1, 2 and 5 hours after infiltration and flash-frozen in liquid N_2. Samples were homogenized with zirconium beads (1.4 mm diameter) using a Bead Ruptor equipped with a cooling unit (Omni International, Kennesaw, GA, USA). Total RNA isolation was performed using GENEzol reagent (Geneaid Biotech, Taipei, Taiwan) following the manufacturer's instructions. DNA contamination was removed using the on-column DNase treatment of the RNase-Free DNase Set (Qiagen GmbH, Hilden, Germany). Concentration and quality were measured by Qubit fluorometer (Life Technologies) and Tapestation (Agilent). Library

preparations and sequencing were performed at the Functional Genomics Center Zurich (http://www.fgcz.ch/). Ribosomal RNA was depleted by poly-A enrichment and DNA libraries were sequenced. The library preparation was performed with Illumina's TruSeq Stranded mRNA kit using 500 ng of total RNA as input amount. The sequencing of the resulting libraries was performed on Illumina NovaSeq 6000 in single read 100 bp mode.

RNA-seq analysis

Raw Illumina reads were pseudo-aligned to the wheat transcriptome (release 41 on https://plants.ensembl.org/, accessed November 2018) and to the *Z. tritici* transcriptome (Accession number PRJNA290690 on https://www.ncbi.nlm.nih.gov/, accessed November 2018) using Kallisto v0.44.00 (Bray et al. 2016; Supplementary Table S3). Read counts were then imported into R using the R-package tximport (Soneson et al. 2015; RStudio 2020). Normalization for RNA composition was performed with the edgeR package (Robinson et al. 2010) using the function calcNormFactors, and dispersion was estimated using the following functions: estimateGLMCommonDisp, estimateGLMTrendedDisp, and estimateGLMTagwiseDisp. For both wheat and *Z. tritici,* a gene was considered expressed if the counts per million (cpm) were >5 in at least 3 out of the 18 replicates, as described (Poretti et al. 2021).

Differential gene expression analyses were performed using both edgeR (Robinson et al. 2010) and DESeq2 (Love et al. 2014). For edgeR, the pipeline described (Praz et al. 2017) was followed. A negative binomial generalized log-linear model has been fitted to the read count for each gene using the glmFit function, and we tested for differential expression with the glmLRT function with different contrasts for pairwise

591 comparisons. In DESeq2, standard parameters were used. Genes with a $log_2FC > |1.5|$
592 and an adjusted p-value (FDR) < 0.01 in both approaches (DESeq2 and edgeR) were
593 included in the final set of differentially expressed genes (DEGs; Supplementary Table
594 S4). Various pairwise comparisons were performed between infiltrated or infected
595 samples against the corresponding control. The different pairwise comparisons are
596 described in Supplementary Table S5. All raw sequence data generated in this study
597 have been deposited in the NCBI Sequence Read Archive under accession number
598 GSE250605.

599 **Lists of the genes of interest and their functional annotation**

600 To functionally annotate the genes identified as DE in wheat, GO annotations were
601 retrieved from Ensembl using the R package BiomaRt (Durinck et al. 2009), and GO
602 enrichment analyses were performed for the "DEGs in infiltration", the "Core DEGs",
603 the "3D7+AvrStb6$_{1E4}$-specific DEGs'' and the "3D7-specific DEGs'' using topGO (Alexa
604 and Rahnenfuhrer 2022). GO terms identified as enriched in any of the lists of genes of
605 interest were manually classified into different categories according to their biological
606 functions (Supplementary Table S6). To functionally annotate the "AvrStb6 specific
607 genes'', we used Uniprot (https://www.uniprot.org/) and performed blast searches
608 against the conserved domain database (CDD, https://www.ncbi.nlm.nih.gov/cdd/)
609 using standard parameters (Supplementary Tables S8, S9 and S10). Stomata related
610 genes and NADPH oxidase genes were identified by BLAST using the Arabidopsis
611 sequence as a query. To identify secreted proteins and effector candidates in the DEGs
612 in *Z. tritici*, the protein sequences of all the genes identified as DE in each comparison

613 have been analyzed using SignalP version 6.0 (Teufel et al. 2022) and EffectorP version

614 3.0 (Sperschneider and Dodds 2022).

615

ACKNOWLEDGEMENTS

We thank Sreedhar Kilaru and Gero Steinberg for providing pCmCherry, pCZtGFP, and strains 3D7 and 1E4 expressing GFP; and Kostya Kanyuka for providing Bobwhite and Bobwhite+Stb6. Seeds of cultivars Runal and Chinese Spring were kindly purchased from DSP Ltd. (Delley, Switzerland). We thank Jason Rudd for providing pCGEN. Confocal laser scanning microscopy experiments were supported by the Scientific Center for Optical and Electron Microscopy (ScopeM), ETH Zurich. RNA extraction and RNAs-eq analysis were performed in collaboration with the Genetic Diversity Center (GDC), ETH Zurich. RNA sequencing was conducted in the Functional Genomics Center Zurich (FGCZ).

This work was supported by the Ministry of Science and Innovation (Grant PID2019-108693RA-I00 to ASV). ASV was the recipient of the RYC2018-025530-I grant from the Spanish Ministry of Science, Innovation and Universities. CP was a recipient of the Early Postdoc. Mobility-Grant, Nr. P2ZHP3_195287, from the Swiss National Science Foundation. ADF obtained the "*Ayudas María Zambrano para la atracción de talento internacional*" Postdoctoral Fellowship from the Ministry of Universities of the Spanish government and the European Union Next Generation EU. CCL was financially supported by the 'Severo Ochoa (SO) Programme for Centres of Excellence in R&D' from the Agencia Estatal de Investigación of Spain (grant CEX2020-000999-S (2022-2025) to the CBGP).

References

Alexa, A., and Rahnenfuhrer, J. 2022. topGO: Enrichment analysis for gene ontology. 10.18129/B9.bioc.topGO.

Arraiano, L. S., and Brown, J. K. M. 2006. Identification of isolate-specific and partial resistance to septoria tritici blotch in 238 European wheat cultivars and breeding lines. Plant Pathol. 55:726–738.

Barrett, L. G., Zala, M., Mikaberidze, A., Alassimone, J., Ahmad, M., McDonald, B. A., et al. 2021. Mixed infections alter transmission potential in a fungal plant pathogen. Environ. Microbiol. 23:2315–2330.

Battache, M., Lebrun, M.-H., Sakai, K., Soudière, O., Cambon, F., Langin, T., et al. 2022. Blocked at the stomatal gate, a key step of wheat Stb16q-mediated resistance to *Zymoseptoria tritici*. Front. Plant Sci. 13.

Bernasconi, A., Lorrain, C., Flury, P., Alassimone, J., McDonald, B. A., and Sánchez-Vallet, A. 2023. *Zymoseptoria tritici* suppresses the host immune response and2 facilitates the success of avirulent strains in mixed infections. PLOS Pathogens 19(11): e1011767.

Brandt, B., Brodsky, D. E., Xue, S., Negi, J., Iba, K., Kangasjärvi, J., et al. 2012. Reconstitution of abscisic acid activation of SLAC1 anion channel by CPK6 and OST1 kinases and branched ABI1 PP2C phosphatase action. Proc. Natl. Acad. Sci. U. S. A. 109:10593–10598.

Bray, N. L., Pimentel, H., Melsted, P., and Pachter, L. 2016. Near-optimal probabilistic RNA-seq quantification. Nat. Biotechnol. 34:525–527.

660 Brown, J. K. M., Chartrain, L., Lasserre-Zuber, P., and Saintenac, C. 2015. Genetics of
661 resistance to *Zymoseptoria tritici* and applications to wheat breeding. Fungal Genet.
662 Biol. 79:33–41.

663 Brunner, P. C., and McDonald, B. A. 2018. Evolutionary analyses of the avirulence
664 effector AvrStb6 in global populations of *Zymoseptoria tritici* identify candidate amino
665 acids involved in recognition. Mol. Plant Pathol. 19:1836–1846.

666 Chartrain, L., Brading, P. A., and Brown, J. K. M. 2005. Presence of the Stb6 gene for
667 resistance to septoria tritici blotch (*Mycosphaerella graminicola*) in cultivars used in
668 wheat-breeding programmes worldwide. Plant Pathol. 54:134–143.

669 Cohen, L., and Eyal, Z. 1993. The histology of processes associated with the infection of
670 resistant and susceptible wheat cultivars with Septoria tritici. Plant Pathol. 42:737–
671 743.

672 Cook, D. E., Mesarich, C. H., and Thomma, B. P. H. J. 2015. Understanding plant
673 immunity as a surveillance system to detect invasion. Annu. Rev. Phytopathol. 53:541–
674 563.

675 Duncan, K. E., and Howard, R. J. 2000. Cytological analysis of wheat infection by the
676 leaf blotch pathogen *Mycosphaerella graminicola*. Mycol. Res. 104:1074–1082.

677 Durinck, S., Spellman, P. T., Birney, E., and Huber, W. 2009. Mapping identifiers for the
678 integration of genomic datasets with the R/Bioconductor package biomaRt. Nat.
679 Protoc. 4:1184–1191.

680 Flütsch, S., Nigro, A., Conci, F., Fajkus, J., Thalmann, M., Trtílek, M., et al. 2020. Glucose
681 uptake to guard cells via STP transporters provides carbon sources for stomatal

682 opening and plant growth. EMBO 21:e49719.

683 Fones, H., and Gurr, S. 2015. The impact of Septoria tritici Blotch disease on wheat: An
684 EU perspective. Fungal Genet. Biol. 79:3–7.

685 Fones, H. N., Eyles, C. J., Kay, W., Cowper, J., and Gurr, S. J. 2017. A role for random,
686 humidity-dependent epiphytic growth prior to invasion of wheat by *Zymoseptoria*
687 *tritici*. Fungal Genet. Biol. 106:51–60.

688 Förster, S., Schmidt, L. K., Kopic, E., Anschütz, U., Huang, S., Schlücking, K., et al. 2019.
689 Wounding-induced stomatal closure requires jasmonate-mediated activation of GORK
690 K+ channels by a Ca2+ sensor-kinase CBL1-CIPK5 Complex. Dev. Cell. 48:87-99.e6.

691 Geiger, D., Scherzer, S., Mumm, P., Marten, I., Ache, P., Matschi, S., et al. 2010. Guard
692 cell anion channel SLAC1 is regulated by CDPK protein kinases with distinct Ca2+
693 affinities. Proc. Natl. Acad. Sci. U. S. A. 107:8023–8028.

694 Ghiasi Noei, F., Imami, M., Didaran, F., Ghanbari, M. A., Zamani, E., Ebrahimi, A., et al.
695 2022. Stb6 mediates stomatal immunity, photosynthetic functionality, and the
696 antioxidant system during the *Zymoseptoria tritici*-wheat interaction. Front. Plant Sci.
697 13.

698 Hafeez, A. N., Chartrain, L., Feng, C., Cambon, F., Griffiths, S., Hayta, S., et al. 2023.
699 Septoria tritici blotch resistance gene Stb15 encodes a lectin receptor-like kinase 1.
700 bioRxiv 1–22.

701 Haueisen, J., Möller, M., Eschenbrenner, C. J., Grandaubert, J., Seybold, H., Adamiak,
702 H., et al. 2019. Highly flexible infection programs in a specialized wheat pathogen. Ecol.
703 Evol. 9:275–294.

704 Jones, J. D. G., and Dangl, J. L. 2006. The plant immune system. Nature. 444:323–329.

705 Kadota, Y., Sklenar, J., Derbyshire, P., Stransfeld, L., Asai, S., Ntoukakis, V., et al. 2014.
706 Direct Regulation of the NADPH Oxidase RBOHD by the PRR-Associated Kinase BIK1
707 during Plant Immunity. Mol. Cell. 54:43–55.

708 Kanyuka, K., and Rudd, J. J. 2019. Cell surface immune receptors: the guardians of the
709 plant's extracellular spaces. Curr. Opin. Plant Biol. 50:1–8.

710 Kema, G. H. J., Mirzadi Gohari, A., Aouini, L., Gibriel, H. A. Y., Ware, S. B., van den
711 Bosch, F., et al. 2018. Stress and sexual reproduction affect the dynamics of the wheat
712 pathogen effector AvrStb6 and strobilurin resistance. Nat. Genet. 50:375–380.

713 Kema, G. H. J., Yu, D., Rijkenberg, F. H. J., Shaw, M. W., and Baayen, R. P. 1996.
714 Histology of the pathogenesis of *Mycosphaerella graminicola* in wheat.
715 Phytopathology. 86:777–786.

716 Kilaru, S., Schuster, M., Studholme, D., Soanes, D., Lin, C., Talbot, N. J., et al. 2015. A
717 codon-optimized green fluorescent protein for live cell imaging in *Zymoseptoria tritici*.
718 Fungal Genet. Biol. 79:125–131.

719 Kong, D., Hu, H. C., Okuma, E., Lee, Y., Lee, H. S., Munemasa, S., et al. 2016. L-Met
720 activates Arabidopsis GLR Ca2+ channels upstream of ROS production and regulates
721 stomatal movement. Cell Rep. 17:2553–2561.

722 Krattinger, S. G., and Keller, B. 2016. Molecular genetics and evolution of disease
723 resistance in cereals. New Phytol. 212:320–332.

724 Kwak, J. M., Mori, I. C., Pei, Z. M., Leonhard, N., Angel Torres, M., Dangl, J. L., et al.
725 2003. NADPH oxidase AtrbohD and AtrbohF genes function in ROS-dependent ABA

726 signaling in arabidopsis. EMBO J. 22:2623–2633.

727 Linde, C. C., Zhan, J., and McDonald, B. A. 2002. Population structure of
728 *Mycosphaerella graminicola*: from lesions to continents. Phytopathology. 92:946–955.

729 Liu, Y., Maierhofer, T., Rybak, K., Sklenar, J., Breakspear, A., Johnston, M. G., et al.
730 2019. Anion channel SLAH3 is a regulatory target of chitin receptor-associated kinase
731 PBL27 in microbial stomatal closure. Elife. 8:1–23.

732 Love, M. I., Huber, W., and Anders, S. 2014. Moderated estimation of fold change and
733 dispersion for RNA-seq data with DESeq2. Genome Biol. 15:550.

734 Meile, L., Croll, D., Brunner, P. C., Plissonneau, C., Hartmann, F. E., McDonald, B. A., et
735 al. 2018. A fungal avirulence factor encoded in a highly plastic genomic region triggers
736 partial resistance to septoria tritici blotch. New Phytol. 219:1048–1061.

737 Meile, L., Peter, J., Puccetti, G., Alassimone, J., McDonald, B. A., and Sánchez-Vallet, A.
738 2020. Chromatin dynamics contribute to the spatiotemporal expression pattern of
739 virulence genes in a fungal plant pathogen. MBio. 11.

740 Meile, L., Garrido-Arandia, M., Bernasconi, Z., Peter, J., Schneller, A., Bernasconi, A., et
741 al. 2023. Natural variation in Avr3D1 from *Zymoseptoria* sp. contributes to quantitative
742 gene-for-gene resistance and to host specificity. New Phytol. 238:1562–1577.

743 Melotto, M., Zhang, L., Oblessuc, P. R., and He, S. Y. 2017. Stomatal defense a decade
744 later. Plant Physiol. 174:561–571.

745 Menna, A., Dora, S., Sancho-Andrés, G., Kashyap, A., Meena, M. K., Sklodowski, K., et
746 al. 2021. A primary cell wall cellulose-dependent defense mechanism against vascular
747 pathogens revealed by time-resolved dual transcriptomics. BMC Biol. 19:161.

748 Meyer, S., Mumm, P., Imes, D., Endler, A., Weder, B., Al-Rasheid, K. A. S., et al. 2010.
749 AtALMT12 represents an R-type anion channel required for stomatal movement in
750 Arabidopsis guard cells. Plant J. 63:1054–1062.

751 Molina, A., Miedes, E., Bacete, L., Rodríguez, T., Mélida, H., Denancé, N., et al. 2021.
752 Arabidopsis cell wall composition determines disease resistance specificity and fitness.
753 Proc. Natl. Acad. Sci. U. S. A. 118.

754 Motteram, J., Lovegrove, A., Pirie, E., Marsh, J., Devonshire, J., van de Meene, A., et al.
755 2011. Aberrant protein N-glycosylation impacts upon infection-related growth
756 transitions of the haploid plant-pathogenic fungus *Mycosphaerella graminicola*. Mol.
757 Microbiol. 81:415–433.

758 Mustilli, A.-C., Merlot, S., Vavasseur, A., Fenzi, F., and Giraudat, J. 2002. Arabidopsis
759 OST1 protein kinase mediates the regulation of stomatal aperture by abscisic acid and
760 acts upstream of reactive oxygen species production. Plant Cell. 14:3089–3099.

761 Negi, J., Matsuda, O., Nagasawa, T., Oba, Y., Takahashi, H., Kawai-Yamada, M., et al.
762 2008. CO2 regulator SLAC1 and its homologues are essential for anion homeostasis in
763 plant cells. Nature. 452:483–486.

764 O'Driscoll, A., Kildea, S., Doohan, F., Spink, J., and Mullins, E. 2014. The wheat–septoria
765 conflict: a new front opening up? Trends Plant Sci. 19:602–610.

766 Palma-Guerrero, J., Ma, X., Torriani, S. F. F., Zala, M., Francisco, C. S., Hartmann, F. E.,
767 et al. 2017. Comparative transcriptome analyses in *Zymoseptoria tritici* reveal
768 significant differences in gene expression among strains during plant infection. Mol.
769 Plant-Microbe Interact. 30:231–244.

770 Poretti, M., Sotiropoulos, A. G., Graf, J., Jung, E., Bourras, S., Krattinger, S. G., et al.
771 2021. Comparative transcriptome analysis of wheat lines in the field reveals multiple
772 essential biochemical pathways suppressed by obligate pathogens. Front. Plant Sci. 12.

773 Praz, C. R., Bourras, S., Zeng, F., Sánchez-Martín, J., Menardo, F., Xue, M., et al. 2017.
774 *AvrPm2* encodes an RNase-like avirulence effector which is conserved in the two
775 different specialized forms of wheat and rye powdery mildew fungus. New Phytol.
776 213:1301–1314.

777 Robinson, M. D., McCarthy, D. J., and Smyth, G. K. 2010. edgeR: a Bioconductor
778 package for differential expression analysis of digital gene expression data.
779 Bioinformatics. 26:139–140.

780 RStudio, P. 2020. RStudio: Integrated Development for R. http://www.rstudio.com/.

781 Rudd, J. J., Kanyuka, K., Hassani-Pak, K., Derbyshire, M., Andongabo, A., Devonshire, J.,
782 et al. 2015. Transcriptome and metabolite profiling of the infection cycle of
783 *Zymoseptoria tritici* on wheat reveals a biphasic interaction with plant immunity
784 involving differential pathogen chromosomal contributions and a variation on the
785 hemibiotrophic lifestyle definition. Plant Physiol. 167:1158–1185.

786 Sacristán, S., and García-Arenal, F. 2008. The evolution of virulence and pathogenicity
787 in plant pathogen populations. Mol. Plant Pathol. 9:369–84.

788 Saintenac, C., Cambon, F., Aouini, L., Verstappen, E., Ghaffary, S. M. T., Poucet, T., et al.
789 2021. A wheat cysteine-rich receptor-like kinase confers broad-spectrum resistance
790 against septoria tritici blotch. Nat. Commun. 12:433.

791 Saintenac, C., Lee, W.-S., Cambon, F., Rudd, J. J., King, R. C., Marande, W., et al. 2018.

792 Wheat receptor-kinase-like protein Stb6 controls gene-for-gene resistance to fungal
793 pathogen *Zymoseptoria tritici*. Nat. Genet. 50:368.

794 Sánchez-Vallet, A., Fouché, S., Fudal, I., Hartmann, F. E., Soyer, J. L., Tellier, A., et al.
795 2018. The genome biology of effector gene evolution in filamentous plant pathogens.
796 Annu. Rev. Phytopathol. 56:21–40.

797 Sánchez-Vallet, A., McDonald, M. C., Solomon, P. S., and McDonald, B. A. 2015. Is
798 *Zymoseptoria tritici* a hemibiotroph? Fungal Genet. Biol. 79:29–32.

799 Sasaki, T., Mori, I. C., Furuichi, T., Munemasa, S., Toyooka, K., Matsuoka, K., et al. 2010.
800 Closing plant stomata requires a homolog of an aluminum-activated malate
801 transporter. Plant Cell Physiol. 51:354–365.

802 Scherzer, S., Maierhofer, T., Al-Rasheid, K. A. S., Geiger, D., and Hedrich, R. 2012.
803 Multiple calcium-dependent kinases modulate ABA-activated guard cell anion
804 channels. Mol. Plant. 5:1409–1412.

805 Schneider, C. A., Rasband, W. S., and Eliceiri, K. W. 2012. NIH Image to ImageJ: 25 years
806 of image analysis. Nat. Methods. 9:671–675.

807 Soneson, C., Love, M. I., and Robinson, M. D. 2015. Differential analyses for RNA-seq:
808 transcript-level estimates improve gene-level inferences. F1000Research. 4:1521.

809 Sperschneider, J., and Dodds, P. N. 2022. EffectorP 3.0: Prediction of apoplastic and
810 cytoplasmic effectors in fungi and oomycetes. Mol. Plant-Microbe Interact. 35:146–
811 156.

812 Steinberg, G. 2015. Cell biology of *Zymoseptoria tritici*: Pathogen cell organization and
813 wheat infection. Fungal Genet. Biol. 79:17–23.

814 Stephens, C., Ölmez, F., Blyth, H., McDonald, M., Bansal, A., Turgay, E. B., et al. 2021.
815 Remarkable recent changes in the genetic diversity of the avirulence gene *AvrStb6* in
816 global populations of the wheat pathogen *Zymoseptoria tritici*. Mol. Plant Pathol.
817 22:1121–1133.

818 Tang, D., Wang, G., and Zhou, J.-M. 2017. Receptor Kinases in Plant-Pathogen
819 Interactions: More Than Pattern Recognition. Plant Cell. 29:618–637.

820 Teufel, F., Almagro Armenteros, J. J., Johansen, A. R., Gíslason, M. H., Pihl, S. I., Tsirigos,
821 K. D., et al. 2022. SignalP 6.0 predicts all five types of signal peptides using protein
822 language models. Nat. Biotechnol. 40:1023–1025.

823 Torriani, S. F. F., Melichar, J. P. E., Mills, C., Pain, N., Sierotzki, H., and Courbot, M.
824 2015. *Zymoseptoria tritici*: A major threat to wheat production, integrated approaches
825 to control. Fungal Genet. Biol. 79:8–12.

826 Toruño, T. Y., Stergiopoulos, I., and Coaker, G. 2016. Plant-Pathogen Effectors: Cellular
827 Probes Interfering with Plant Defenses in Spatial and Temporal Manners. Annu. Rev.
828 Phytopathol. 54:419–441.

829 Vahisalu, T., Kollist, H., Wang, Y.-F., Nishimura, N., Chan, W.-Y., Valerio, G., et al. 2008.
830 SLAC1 is required for plant guard cell S-type anion channel function in stomatal
831 signalling. Nature. 452:487–91.

832 Wu, J., and Liu, Y. 2022. Stomata–pathogen interactions: over a century of research.
833 Trends Plant Sci. 27:964–967.

834 Zenkl, R., Anderegg, J., and McDonald, B. 2023. leaf-toolkit (0.1.0) [Computer
835 software]. https://github.com/RadekZenkl/leaf-toolkit

836 Zhan, J., Kema, G. H. J., Waalwijk, C., and McDonald, B. A. 2002. Distribution of mating
837 type alleles in the wheat pathogen *Mycosphaerella graminicola* over spatial scales
838 from lesions to continents. Fungal Genet. Biol. 36:128–136.

839 Zheng, X., Kang, S., Jing, Y., Ren, Z., Li, L., Zhou, J.-M., et al. 2018. Danger-associated
840 peptides close stomata by OST1-independent activation of anion channels in guard
841 cells. Plant Cell. 30:1132–1146.

842 Zhong, Z., Marcel, T. C., Hartmann, F. E., Ma, X., Plissonneau, C., Zala, M., et al. 2017. A
843 small secreted protein in *Zymoseptoria tritici* is responsible for avirulence on wheat
844 cultivars carrying the Stb6 resistance gene. New Phytol. 214:619–631.

845

Figure legends

Figure 1. Recognition of AvrStb6 hinders the penetration of *Zymoseptoria tritici*. Confocal microscopy images of wheat cultivar Chinese Spring sprayed with the *Z. tritici* cytosolic reporter lines 3D7 (3D7-GFP; A-C and G) and 1E4 (1E4-GFP; D-F and H). **A**. At 6 days post-infection (dpi), the virulent strain 3D7 penetrated the leaf apoplast. **B.** At 10 and **C.** 14 dpi, 3D7 invaded the leaf apoplastic space and accumulated in sub-stomatal cavities. **D-F**. The avirulent strain remained at the leaf surface at all observed timepoints (6, 10, and 14 dpi; D, E and F, respectively). **G,H.** Stomata close-up views of compatible (G) and incompatible (H) interactions observed at 6 dpi. Images A-H are maximum projections, and A'-H' are orthogonal views. Dashed lines indicate the location of the orthogonal view on the corresponding image. Images are overlays of GFP signal (green), chloroplast autofluorescence (blue) and plant cells stained with propidium iodide (pink). Full and empty white triangles highlight epiphyllous and apoplastic hyphae, respectively. Scale bar: 20 µm.

Figure 2. AvrStb6 is produced and accumulates at the infection site. A-B. Microscopy images of wild-type Bobwhite plants infected with the 3D7 mCherry-labelled *Zymoseptoria tritici* (red) strain expressing AvrStb6$_{1E4}$ fused to GFP (AvrStb6$_{1E4}$-GFP, green). Observations made at 6 days post-infection (dpi) of hyphae growing epiphytically (A) and in the apoplastic space (B). Images show GFP signal (green), mCherry signal (red) and chloroplast autofluorescence (blue). Images on A and B are maximum projections. Full and empty white triangles highlight epiphyllous and penetrated hyphae, respectively. Scale bar: 20 µm.

Figure 3. **AvrStb6 is a secreted protein**. **A.** Protein alignment of 3D7 (virulent, $AvrStb6_{3D7}$) and 1E4 (avirulent $AvrStb6_{3D7}$) AvrStb6 protein isoforms of *Zymoseptoria tritici*. The red line indicates the predicted signal peptide. Blue boxes highlight amino acid polymorphism. **B.** Subcellular localization of $AvrStb6_{1E4}$-GFP on epiphytic hyphae reaching a stomate of a wild-type Bobwhite plant infected with the 3D7 mCherry-labelled *Z. tritici* strain expressing $AvrStb6_{1E4}$-GFP. Observations made at 6 days post-infection (dpi). Line charts indicate GFP (green) and mCherry (red) signal intensities (absolute grey value) distributed across the lines depicted in the corresponding image. Image is a maximum projection on the overlay of GFP signal (green), mCherry (red) signal, and chloroplast autofluorescence (blue). Observations made at 6dpi. Scale bar: 20 µm. **C.** Western blot analysis of *in-vitro* grown *Z. tritici* 3D7 strains expressing either a cytosolic GFP or each AvrStb6 isoform fused to GFP (3D7+$AvrStb6_{1E4}$-GFP and 3D7+$AvrStb6_{3D7}$-GFP). Fungal lines were grown in liquid media, and the western blot was performed on filtered supernatant (SN; secreted protein) and washed pellet (with and without urea treatment; non-secreted proteins, insoluble fraction) using an anti-GFP antibody. The expected molecular weights of GFP and the AvrStb6-GFP protein fusions are 26.94 and 36 kD, respectively.

Figure 4. AvrStb6 induces an immune response in Stb6-expressing wheat plants. A. AvrStb6 produced in *Pichia pastoris* induces an immune response in the cultivar Chinese Spring and prevents the infection of *Zymoseptoria tritici* strain 3D7. AvrStb6 was infiltrated in Chinese Spring plants. Plants were subsequently treated with mock or with *Z. tritici* 3D7 spore suspension. Pictures were taken 11 days after infection. Virulence is estimated as percentages of leaf area covered by lesions (PLACL). **B.**

Barplot showing the number of differentially expressed genes (DEGs) in wheat upon AvrStb6 infiltration compared to the PBS control at three different timepoints (1 hour post infiltration (hpi), 2hpi and 5 hpi). **C.** Intersection plot showing the overlap between the different sets of DEGs. Colors of bars in the right panel correspond to genes differentially expressed at the three timepoints (light grey), at two timepoints (dark grey) or at only one timepoint (black). **D.** Expression levels (log2 fold-change compared to PBS) of stomatal closure-related genes differentially up-regulated upon AvrStb6 infiltration at 5 hpi (log2 fold change >1.5; FDR < 0.01). Expression patterns of *ALMT12* (TraesCS1A02G189900), *OST1* (TraesCS1B02G281100), *PBL27* (TraesCS2D02G079200), 1 *CPK* (TraesCS5B02G428400), 1 *RBOH* (TraesCS5D02G222100), and 1 *BIK1* (TraesCS7D02G474600) homologs are shown. The expression values are at 1, 2 and 5 hours post infiltration of the purified AvrStb6. **E.** Barplot showing wheat DEGs upon infection with the virulent strain 3D7 and with the avirulent strain 3D7+AvrStb6$_{1E4}$ compared to mock-treated plants at 3 or 6 days post infection (dpi). **F.** Intersection plots show the overlap between the different sets of DEGs. Colors of bars in the right panel correspond to three sets of genes: grey = core DEGs, orange = 3D7+AvrStb6$_{1E4}$-specific DEGs and green = 3D7-specific DEGs. The rest of the genes are shown in black. **G.** Expression (log2 fold-change compared to mock) at 3 and 6 dpi of stomatal closure-related genes identified in "3D7+AvrStb6$_{1E4}$-specific DEGs" set at 3 dpi. Expression patterns of 1 *RBOH* (TraesCS1B02G362200), *SLAC1* (TraesCS3D02G228400), 1 *CPK* (TraesCS4A02G206200), and 1 *BIK1* (TraesCS7B02G473700) homologs are shown. Genes shown are differentially expressed upon infection with the avirulent strain compared to the mock (log2 fold change >1.5; FDR < 0.01), but not with the virulent strain.

Figure 5. Defense-related genes contribute to AvrStb6-specific response in wheat. A. Venn diagram representing the overlap between the differentially expressed genes identified in the different pairwise comparisons: infiltration of AvrStb6 compared to control (PBS), infection with 3D7 compared to the mock treatment, and infection with the avirulent strain 3D7+AvrStb6$_{1E4}$ compared to the mock treatment. The highlighted 247 genes correspond to the genes responding specifically to the presence of AvrStb6. **B.** Heatmap of the 247 genes differentially expressed in the presence of AvrStb6 in both the spray infection and infiltration experiments. The log2 fold change is represented for each pairwise comparison. In the left column, black bars indicate the genes containing protein domains linked to defense responses. **C.** Expression pattern of an *MLO* (*TraesCS1B02G272200*) and 10 *RLKs* within the 247 genes (differentially expressed upon infiltration with AvrStb6 protein and infection with 3D7+AvrStb61E4, but not with 3D7). Top panel: log2 fold change expression upon infiltration of AvrStb6 at 1, 2, and 5 hours post-infiltration (hpi). Bottom panel: log2 fold change expression upon infection with the wildtype strain (3D7) and the avirulent strain (3D7+AvrStb6) compared to mock at 3 and 6 days post-infection (dpi).

Figure 6. The avirulent AvrStb6 expressing strain is blocked at the early stages of the infection. A. Multidimensional scaling (MDS) plot of the expression data of *Zymoseptoria tritici* virulent (3D7) and avirulent (3D7+AvrStb6$_{1E4}$) strains, during infection of the resistant cultivar Chinese Spring at 3 and 6 days post-infection (dpi). The different colors correspond to different treatments (green = 3D7 and orange = 3D7+AvrStb6$_{1E4}$), representing the two timepoints with different shapes. **B.** Barplots

943 showing the number of differentially expressed genes (DEGs) between strains (light
944 orange) and between timepoints (light green). Light grey represents genes encoding
945 not-secreted proteins, and dark grey genes encoding secreted proteins. **C.** Intersection
946 plots showing the overlap between the different sets of DEGs (Green: between time
947 points for each strain; Orange: between strains at each time point). **D.** Summary of the
948 DEGs identified in the different comparisons and the percentage of secreted proteins
949 and effector genes.
950
951 **Supplementary Figure S1. Virulence assays of the mutant lines obtained in this work.**
952 **A**. Virulence estimated as percentage of leaf area covered by lesions (PLACL) of 3D7-
953 mCherry lines expressing AvrStb6 alleles from 3D7 or 1E4 (*AvrStb6*$_{3D7}$ or *AvrStb6*$_{1E4}$)
954 fused to GFP on Chinese Spring and Drifter wheat cultivars. 1E4, 3D7-mCherry, and
955 mock treatments are shown as controls. **B** Virulence (estimated as PLACL) of 3D7-GFP
956 expressing the avirulent *AvrStb6* allele from 1E4 (3D7-GFP_AvrStb6$_{1E4}$ lines A1 and line
957 A2) on wheat plants cultivars Chinese Spring and Drifter. 1E4, 3D7-GFP, and mock were
958 included as controls. **C** Virulence assay of 1E4 strain on the wild-type Bobwhite cultivar
959 and two independent lines (T2_19-2 and T2_41-4) of Bobwhite expressing Stb6.
960 Expected compatible and incompatible interactions are highlighted in brown and
961 green, respectively. Dark and light colors indicate the transformant lines and the
962 background lines, respectively. The number of leaves analyzed is indicated for each
963 condition (n number).
964
965 **Supplementary Figure S2. Rare events of penetration of *Z. tritici* in an incompatible**
966 **interaction.** Confocal microscopy images of Chinese Spring sprayed with the *Z. tritici*

967 cytosolic reporter line 1E4 (1E4-GFP). **A**. At 10 days post-infection (dpi), rare events of
968 1E4 having penetrated the leaf through stomata can be observed. Apoplastic hyphae
969 remain in close proximity to the penetration site. **B.** At 14 dpi fungal progression in the
970 apoplast remains very limited. Images A and B are maximum projections, A' and B' are
971 orthogonal views. Dashed lines indicate the location of the orthogonal view on the
972 corresponding image. Images are overlays of GFP signal (green), chloroplast
973 autofluorescence (blue), and plant cell walls stained with propidium iodide (pink). Full
974 and empty white triangles highlight epiphyllous and penetrated hyphae, respectively.
975 Scale bar: 20 µm.
976
977 **Supplementary Figure S3. Recognition of AvrStb6 hinders the penetration of *Z. tritici*.**
978 **A-F**. Confocal microscopy images of wheat cultivar Chinese Spring sprayed with *Z. tritici*
979 3D7-GFP and 3D7-GFP expressing AvtStb6$_{1E4}$ (3D7-GFP+AvrStb6$_{1E4}$). **A,B.** At 6 days
980 post-infection (dpi, A), the virulent strain 3D7 penetrated the leaf and started invading
981 its apoplastic space. At later stages (10 dpi, B), 3D7 invaded the leaf apoplast and
982 accumulated in sub-stomatal cavities. **C-F**. 3D7-GFP reporter line ectopically expressing
983 the *AvrStb6$_{1E4}$* gene does not penetrate through the stomata of Chinese Spring plants
984 at 6 dpi (C, E) and at 10 dpi (D, F). Images of two independent transformant lines (Line
985 A1 shown in C and D, and line A2 shown in E and F) depict identical observations. **G-L**.
986 Confocal microscopy images of *Z. tritici* cytosolic reporter lines 1E4 (1E4-GFP) sprayed
987 on Bobwhite and Bobwhite expressing the wheat resistance gene, *Stb6*. At 6 and 9 dpi,
988 1E4 penetrated and colonized the apoplast of Bobwhite (**G, H**). However, it remained
989 at the leaf surface when inoculated on the Bobwhite expressing *Stb6* (**I-L**). Images of
990 two independent wheat transformant lines (T2-19-2 shown in I and K, and T2-41-4

991 shown in J and L) depict identical observations at both 6 and 9 dpi. Rare instances of
992 penetration could be observed, but those events present very limited apoplastic
993 hyphal growth (J). Images A-L are maximum projections, and A'-L' are orthogonal
994 views. Dashed lines indicate the location of the orthogonal view on the corresponding
995 image. Images are overlays of GFP signal (green), chloroplast autofluorescence (blue)
996 and plant cell walls stained with propidium iodide (pink). Full and empty white
997 triangles highlight epiphyllous and penetrated hyphae, respectively. Scale bar: 20 µm.
998
999 **Supplementary Figure S4. AvrStb6 accumulates in hyphal cells in direct contact with**
1000 **stomata. A-D**. Microscopy images of Bobwhite wheat plants infected with *Z. tritici*
1001 reporter line expressing AvrStb6$_{1E4}$-GFP (3D7-mCherry+ AvrStb6$_{1E4}$-GFP) at 6 and 9 days
1002 post-infection (dpi; A-B and C-D, respectively). In epiphytic hyphae, the GFP signal can
1003 only be observed in hyphal cells in direct contact with stomata (A and C). At both 6 and
1004 9 dpi (B and D), hyphae that managed to penetrate through the stomata and colonize
1005 the leaf apoplast accumulate GFP. **E-J**. Bobwhite near-isogenic lines expressing *Stb6*
1006 (T2-19-2 and T2-41-4) were used to observe the AvrStb6$_{1E4}$-GFP localization in the
1007 context of an incompatible interaction. At 6 and 9 dpi (E-G and H-J, respectively), the
1008 AvrStb6$_{1E4}$-GFP signal was observed in hyphal in direct contact with stomata (E-J). Rare
1009 cases of hyphal penetration could be observed (F). In that case, hyphae presented a
1010 faint signal of AvrStb6 accumulation (F'). Images A-F are maximum projection overlays
1011 of GFP signal (green), mCherry signal (red) and chloroplast autofluorescence (blue).
1012 Images on A'-F' are maximum projection overlays of only GFP signal (green) and
1013 chloroplast autofluorescence (blue). **K,L.** Microscopy images illustrating *AvrStb6$_{1E4}$*
1014 expression pattern. The 3D7 mTurquoise-labelled *Z. tritici* strain (in red), expressing a

tagged histone protein (His1-mCherry) under the control of *AvrStb6*$_{1E4}$ promoter, was sprayed on Runal wheat leaves. Fungal nuclei accumulating His1-mCherry signal (in green) indicate cells exhibiting *AvrStb6*$_{1E4}$ promoter activity. Images were acquired at 6 and 9 dpi (K and L, respectively). Epiphytic hyphae show low expression levels of *AvrStb6*, except when the cells approach the stomata. In contrast, apoplastic hyphae strongly express *AvrStb6*. Full and empty white triangles highlight epiphyllous and penetrated hyphae, respectively. Scale bar: 20 µm.

Supplementary Figure S5. Detection of AvrStb6$_{1E4}$ protein produced in *Pichia pastoris*.

AvrStb6$_{1E4}$, coupled with Myc and His tags, was produced in *P. pastoris* and purified using Ni-NTA agarose beads. **A**. Western blot analysis of the AvrStb6$_{1E4}$-Myc-His elutions fractions, separated by SDS-PAGE, and detected using an anti-His antibody. **B**. Coomassie Blue staining (left) and anti-His western blot detection (right) of the purified AvrStb6$_{1E4}$-Myc-His, after Buffer exchange. Lane1: Precision plus protein ladder (5µl). Lane 2: AvrStb6$_{1E4}$-Myc-His (20µl). The expected protein size is 18,5kDa.

Supplementary Figure S6. Overall wheat gene expression pattern upon infiltration and spray infection. A. Multidimensional scaling (MDS) plots of the expression data of 36 wheat RNASeq samples. The different colors correspond to different treatments, and the different shapes to different timepoints. **B.** MDS plot of the expression data of Chinese Spring leaves infiltrated with AvrStb6 protein and PBS buffer at three different timepoints (1 hours post infiltration (hpi), 2 hpi and 5 hpi). The different colors correspond to different treatments (dark blue = infiltrated with PBS buffer, dark

orange = infiltrated with the AvrStb6 protein), and the three timepoints, 1, 2 and 5 hours post infiltration (hpi), are represented with different shapes. **C.** MDS plot of the expression data of Chinese Spring infected with the virulent strain 3D7, the avirulent strain 3D7+AvrStb6$_{1E4}$ or mock at 3 or 6 days post infection (dpi). The different colors correspond to different treatments (light blue = mock, green = infected with 3D7 and orange = infected with 3D7+AvrStb6$_{1E4}$) and the two timepoints are represented with different shapes.

Supplementary Figure S7. Gene Ontology enrichment analysis for the identified sets of differentially expressed genes. The "Biological processes" GO terms for which an enrichment has been observed in any of the gene sets are listed on the y-axis and the x-axis corresponds to the fold enrichment. The size and the color of the circles correspond to the number of genes and to the p-value respectively. GO terms were classified in the following categories: "plant hormones", "photosynthesis, photorespiration, light stimulus and pigments", "cell wall", "stress responses", "secondary metabolism", "cell division, DNA and primary metabolism", and "others".

Supplementary Figure S8. Gene Ontology enrichment analysis in "Molecular Functions" for the identified sets of differentially expressed genes. "Molecular Functions" GO terms for which an enrichment has been observed are listed on the y-axis and the x-axis corresponds to the fold enrichment. The size and the color of the circles correspond to the number of genes and to the p-value, respectively.

Supplementary Figure S9. Gene Ontology enrichment analysis in "Cellular Components" for the identified sets of differentially expressed genes. "Cellular

Components" GO terms for which an enrichment has been observed are listed on the y-axis and the x-axis corresponds to the fold enrichment. The size and the color of the circles correspond to the number of genes and to the p-value, respectively.

Supplementary Table S1. *Zymoseptoria tritici* strains used.

Supplementary Table S2. List of primers used for cloning and quantitative PCR.

Supplementary Table S3. RNASeq read counts statistics. For the 36 RNASeq samples, the percentage of reads mapping to the corresponding CDS as well as the number of reads mapping to the corresponding CDS are indicated.

Supplementary Table S4. Differential gene expression data of all the differential expressed genes in wheat. Gene Length is indicated in column B, counts are indicated for each replicate in columns C to AL. For each pairwise comparison, one column indicated the logFC and one the FDR adjusted p-value (from edgeR). For the infiltration experiment PBS vs AvrStb6 i) at 1hpi in columns AM and AN, ii) at 2hpi in columns AO and AP, iii) at 5hpi in columns AQ and AR. For the spray inoculation mock vs 3D7 iv) at 3dpi in columns AS and AT, v) at 6dpi in columns AU and AV; and mock vs 3D7_AvrStb61E4 vi) at 3dpi in columns AW and AX and vii) at 6dpi in columns AX and AZ. In columns BA to BG, the genes that are differentially expressed in each pairwise comparisons are indicated with "DE". Genes that are part of "DEGs in infiltration", "CORE DEGs", "3D7-specific DEGs" and "3D7_AvrStb61E4" are indicated in columns BH, BI, BJ and BL respectively. Previously cloned resistance genes Stb6, Stb15 and Stb16q are written in red, green and blue respectively.

Supplementary Table S5. Differential gene expression summary. The number of differential expressed genes identified with edgeR and DESeq2 are indicated. The overlap between the two methods has been considered for further analyses.

Supplementary Table S6. List of the biological processes GO terms enriched in enrichment analyses. The GO terms have been classified into categories indicated in columns 3 and 4.

Supplementary Table S7. Differential gene expression data of wheat homolog genes related to stomatal closure. Pairwise comparisons are indicated in columns C to P. For each pairwise comparison, one column indicated the logFC and one the FDR adjusted p-value. In columns Q to W, the genes that are differentially expressed in each pairwise comparisons are indicated with "DE". Genes that are part of "DEGs in infiltration", "CORE DEGs", "3D7-specific DEGs" and "3D7_AvrStb61E4" are indicated in columns X, Y, Z and AA, respectively.

Supplementary Table S8. List of the 247 genes responding specifically to the presence of AvrStb6. Superfamilies for which a hit was obtained when the protein sequence of the gene was blast against the conserved domain database of NCBI are listed in the column "Conserved Protein Domain Family".

Supplementary Table S9. List of the upregulated DEGs among the 247 “AvrStb6-specific genes”, their expression levels and conserved associated domains. List of upregulated genes upon infection with the avirulent strain at 3 dpi considering log2FC >1.5 and FDR <0.01 as shown in the colums J and K respectively (Comp_mock_Avr_3d). Espression levels for the other pairwise comparisons are also shown. infiltration experiment PBS vs AvrStb6 at 1hpi, 2hpi, and 5hpi. For the spray

inoculation, mock vs 3D7 at 3dpi and 6dpi and mock vs 3D7_AvrStb61E4 at 3dpi and 6dpi are included. The following columns are the predicted functions and conserved domains. PANTHER_Family/Subfamily, Protein names UniProt, Protein families, conserved domains, hypothetical functions of each conserved domain, and protein function prediction after putting together the above information. NA= not assigned. Genes highlighted in light green correspond to the ones potentially involved in plant defense response (Supplementary Table S10). Genes highlighted in orange correspond to up-regulated genes encoding proteins involved in cell wall modification. Genes highlighted in blue potentially encode proteins playing a role in stomatal movement, sugar transporter protein (STP), and plant glutamate receptor (GLR).

Supplementary Table S10. Expression levels and protein domain predictions of upregulated genes among the 247 “AvrStb6-specific genes” encoding for proteins involved in plant defense response. For each pairwise comparison, one column indicated the logFC and one the FDR adjusted p-value (from edgeR). For the infiltration experiment PBS vs AvrStb6 i) at 1hpi, ii) at 2hpi, iii) and at 5hpi. For the spray inoculation mock vs 3D7 iv) at 3dpi, v) at 6dpi; and mock vs 3D7_AvrStb61E4 vi) at 3dpi and vii) at 6dpi. All genes in this table are differentially expressed. Genes that are part of "DEGs in infiltration", "CORE DEGs", "3D7-specific DEGs" and "3D7_AvrStb61E4" are indicated with a yes. Functional classification according to PANTHER, Uniprot and conserved domains (CDD, NCBI) are also indicated. The last column shows the biological function assigned to each protein. Abbreviations. RLK: receptor-like kinase; LRR: Leucine-rich repeat; RLP: Receptor-like protein; WAK: Wall-associated kinase; MLO: Mildew resistance locus O; NLR: Nod-like receptor. Genes highlighted in dark green correspond to the ones plotted in Figure 5C.

Supplementary Table S11. Differential gene expression data of all the differential expressed genes in *Z. tritici*. Gene Length is indicated in column B, counts are indicated for each replicate in columns C to N. For each pairwise comparison, one column indicated the logFC and one the FDR adjusted p-value (from edgeR). For the comparisons between isolates (3D7 versus 3D7AvrStb6_1E4) i) at 3dpi in columns O and P and ii) at 6dpi in columns Q and R. For the comparisons between timepoints (3dpi versus 6dpi) iii) in 3D7 in columns S ant T and iv) in 3D7_AvrStb61E4 in columns U and V. In columns W to Z, the genes that are differentially expressed in each pairwise comparisons are indicated with "DE". Genes that contain a signal peptide according to SignalP are listed in column AA and the ones that are effectors according to EffectorP in column AB.

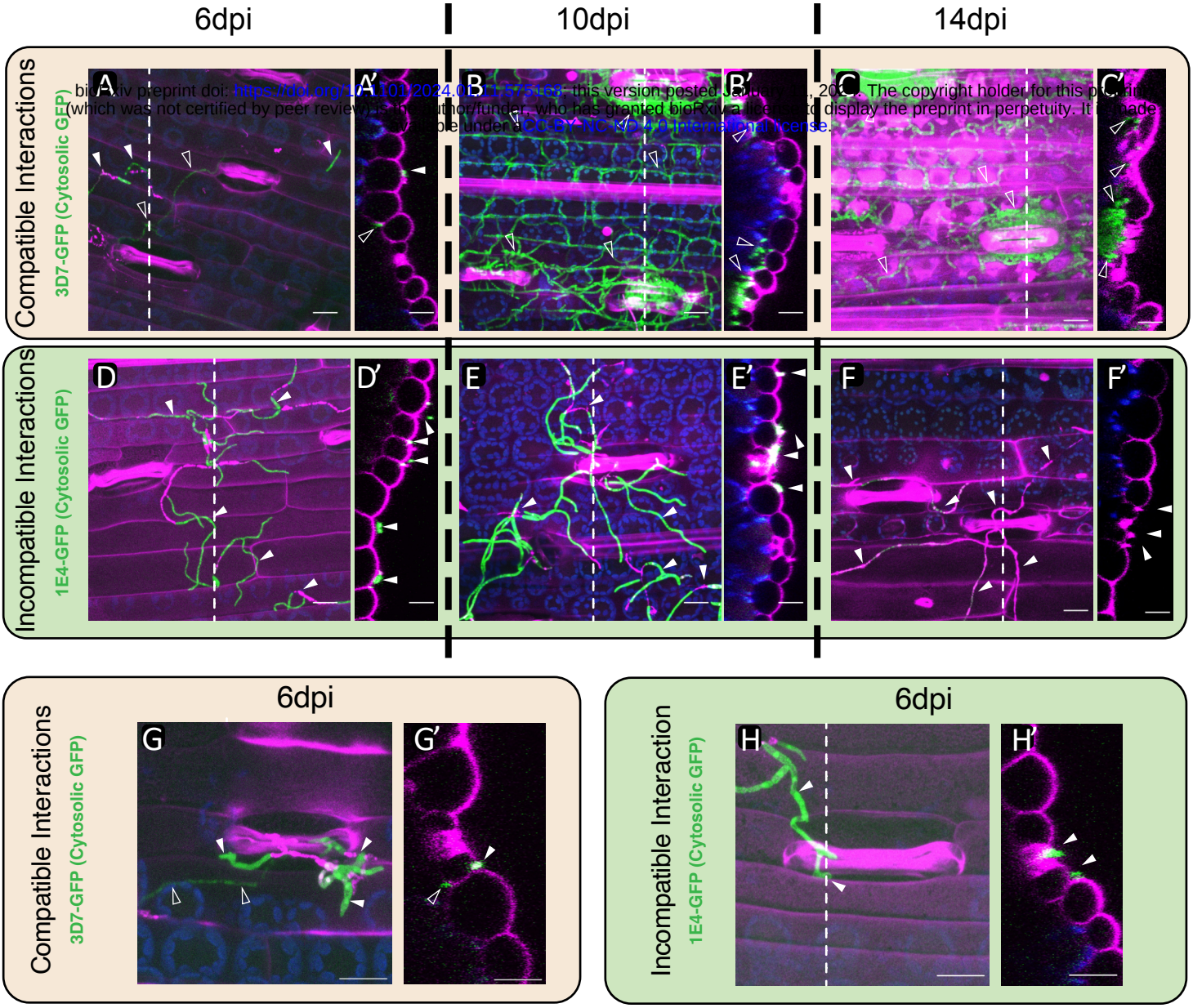

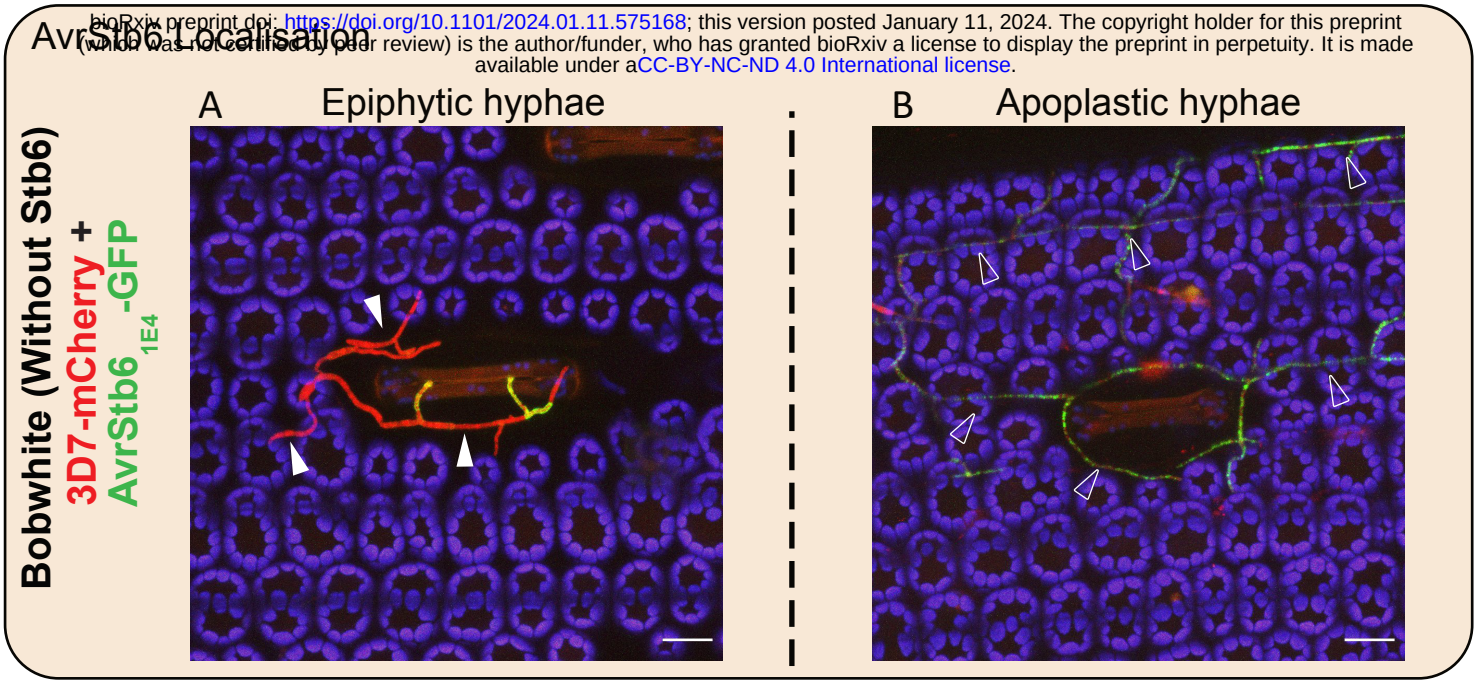

A

```
                    20        40        60        80
AvrStb6_1E4  MRSILQGLLA FALAVGVQAR VVCGGIGDLC KAGPSCCNYP ITNCFQDGQY PRCHTACGNW NFGFCPDGKQ CNCQVILGCG CV*
AvrStb6_3D7  MRSILQGLLA FALAVGVQAR VVCGGIGDLC KAGPSCCNYP ITNCFQDGQY PRCHTACGHF QFGFCHDGKQ CNCQVILGCG CV*
```

B

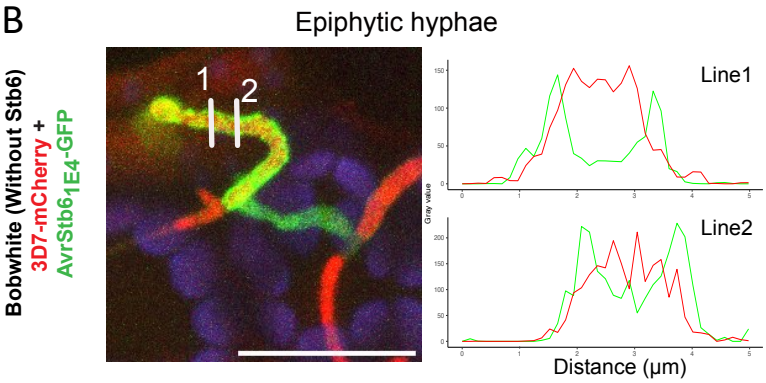

C

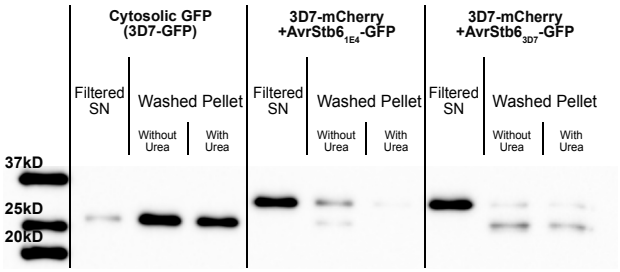

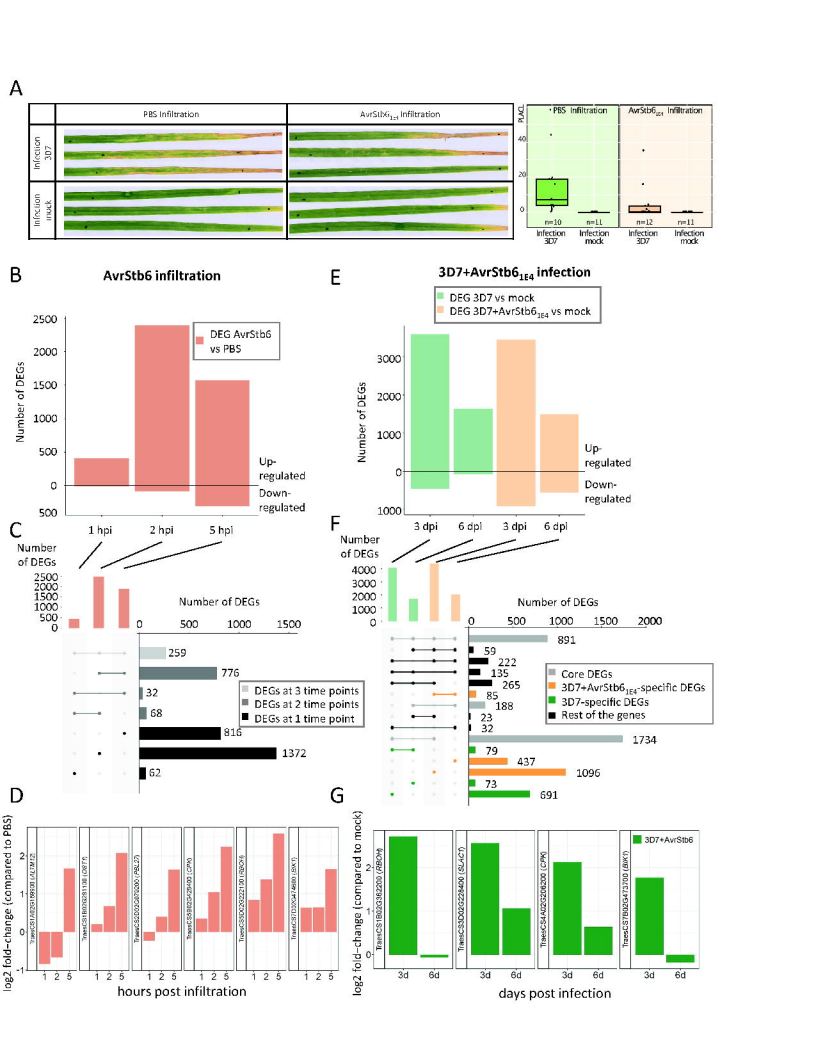
A
PBS Infiltration
AvrStb6 1E4 Infiltration
Infection 3D7
Infection mock
PLACL
PBS Infiltration
AvrStb6 1E4 Infiltration
n=10
n=11
n=12
n=11
Infection 3D7
Infection mock
B
AvrStb6 infiltration
Number of DEGs
DEG AvrStb6 vs PBS
Up-regulated
Down-regulated
1 hpi
2 hpi
5 hpi
C
Number of DEGs
Number of DEGs
259
776
32
68
816
1372
62
DEGs at 3 time points
DEGs at 2 time points
DEGs at 1 time point
D
log2 fold-change (compared to PBS)
hours post infiltration
E
3D7+AvrStb6 1E4 infection
DEG 3D7 vs mock
DEG 3D7+AvrStb6 1E4 vs mock
Number of DEGs
Up-regulated
Down-regulated
3 dpi
6 dpi
3 dpi
6 dpi
F
Number of DEGs
Number of DEGs
891
59
222
135
265
85
188
23
32
1734
79
437
1096
73
691
Core DEGs
3D7+AvrStb6 1E4-specific DEGs
3D7-specific DEGs
Rest of the genes
G
log2 fold-change (compared to mock)
days post infection
3D7+AvrStb6
3d
6d

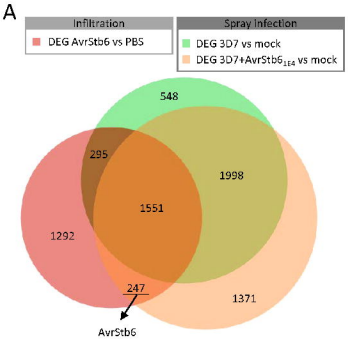
A
Infiltration
DEG AvrStb6 vs PBS
Spray Infection
DEG 3D7 vs mock
DEG 3D7+AvrStb6 1E4 vs mock
548
295
1998
1551
1292
247
1371
AvrStb6
response

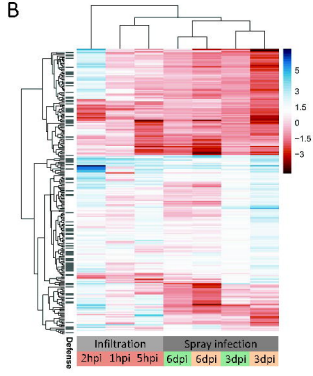
B
5
3
1.5
0
−1.5
−3
Infiltration
Spray infection
2hpi 1hpi 5hpi 6dpi 6dpi 3dpi 3dpi

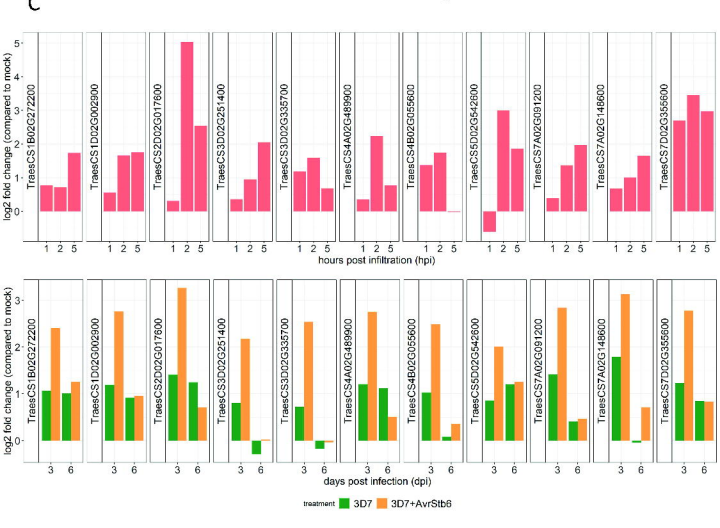
C
log2 fold change (compared to mock)
TraesCS1B02G272200
TraesCS1D02G002900
TraesCS2D02G017600
TraesCS3D02G251400
TraesCS3D02G335700
TraesCS4A02G489900
TraesCS4B02G055600
TraesCS5D02G542600
TraesCS7A02G091200
TraesCS7A02G148600
TraesCS7D02G355600
hours post infiltration (hpi)
days post infection (dpi)
treatment 3D7 3D7+AvrStb6

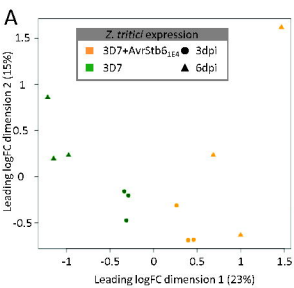

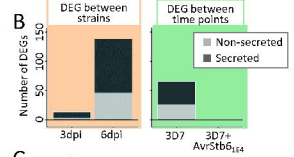

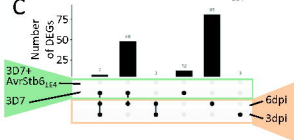

D

Comparison	Number of DEGs	upregulated in 3D7	upregulated in 3D7+AvrStb6IE4	upregulated at 3dpi	upregulated at 6dpi	Non-secreted proteins	Secreted proteins: Non-effector	Secreted proteins: Effector	Percentage of secreted proteins	Percentage of effector
I. Strains										
3D7 vs 3D7+AvrStb6IE4 at 3dpi	13	13	0			3	4	6	77%	46%
3D7 vs 3D7+AvrStb6IE4 at 6dpi	139	138	1			47	34	58	66%	42%
II. Time points										
3dpi vs 6dpi in 3D7	67			2	65	28	18	21	58%	31%
3dpi vs 6dpi in 3D7+AvrStb6IE4	0			0	0					